https://doi.org/10.5194/essd-2026-720
Preprint. Discussion started: 9 November 2026
© Author(s) 2026. CC BY 4.0 License.



Open Access Earth System Science Data Discussions

A national-wide dataset of plot-level living tree biomass and carbon stocks in Chilean native forests

Karen Sandoval-Salazar[1,2], Alejandro Miranda[1,2,3*], Jorge Hoyos-Santillan[2,4,5,6], Rocío Urrutia-Jalabert[1,3,7,8], Timo Tokola[4], Carlos Hormazábal[1,2], Francoise Pincheira[9], Cristian Pérez[9], Blas Mola-Yudego[4]

[1]Departamento de Ciencias Agronómicas y Recursos Naturales, Facultad de Ciencias Agropecuarias y Medioambiente, Universidad de La Frontera, Temuco, Chile.
[2]Laboratorio de Observación de la Tierra y Ecología de Bosques (OB | BO), Temuco, Chile.
[3]Center for Climate and Resilience Research (CR)[2], Santiago, Chile.
[4]School of Forest Sciences, University of Eastern Finland, Joensuu, Finland.
[5]Smithsonian Tropical Research Institute, Panama City, Panama.
[6]School of Biosciences, University of Nottingham, Sutton Bonington, UK.
[7]Millennium Nucleus of Patagonian Limit of Life (LiLi), Chile.
[8]Laboratorio de Dendrocronología y Cambio Global, Instituto de Conservación, Biodiversidad y Territorio, Facultad de Ciencias Forestales y Recursos Naturales, Universidad Austral de Chile, Valdivia, Chile.
[9]Departamento de Monitoreo de Ecosistemas Forestales, Corporación Nacional Forestal (CONAF), Santiago, Chile.

Corresponding to: Alejandro Miranda (alejandro.miranda@ufrontera.cl)

Abstract

Native forests are critical components of the global carbon cycle, yet spatially explicit, national-scale assessments of their aboveground biomass and carbon stocks remain scarce for many regions. Here, we present a harmonized, open-access dataset of a tree-level raw field dataset detailing DBH, height, and species for 59,408 living trees across 77 species derived from 2,024 field plots spanning approximately 2,800 km (30°–56° S). Using these tree-level data, we estimated plot-level aboveground biomass density (AGBd, Mg ha^{-1}) and aboveground carbon density (AGCd, MgC ha^{-1}) for Chilean native forests. Biomass was estimated using a curated set of species-specific allometric equations; for the 29 % of trees falling outside the calibration ranges of their assigned equations, a Boosted Regression Trees (BRT) model was used as a model-assisted estimation approach, and evaluated against held-out allometry-derived biomass (R^2 = 0.979, RMSE = 0.2 in log-space). Results are presented as plot-level estimates by the 12 nationally defined Chilean forest types, three Plant Functional Types (PFTs), three ecoregions, and forest stand development, enabling integration with both national reporting frameworks and global carbon monitoring systems. The Valdivian temperate and Magellanic subantarctic ecoregions store the highest carbon stocks, with primary forest AGBd means of 233-295 Mg ha^{-1} and individual plot values reaching 803.1 Mg ha^{-1} of biomass density and 394.7 MgC ha^{-1} of carbon stock density. The resulting dataset provides a national-scale field-based reference for aboveground biomass and carbon density in Chilean native forests, supporting national carbon assessment, Nationally Determined Contributions (NDCs) under the Paris Agreement, remote-sensing calibration and validation, and long-term forest monitoring of forest carbon dynamics under ongoing climate change. The Plot-level

https://doi.org/10.5194/essd-2026-720
Preprint. Discussion started: 9 November 2026
© Author(s) 2026. CC BY 4.0 License.



Open Access Earth System Science Data Discussions

estimates of living trees carbon stocks in Chilean native forests are publicly available in https://figshare.com/s/d0fbe20f243bad166846.

Keywords: forest biomass, ecological modelling, climate change, nature-based solution, climate strategy

1 Introduction

Forests are central to the global carbon cycle, biodiversity conservation, and the provision of ecosystem services, standing as key nature-based solutions for addressing climate change (Griscom et al., 2017; Seddon et al., 2020). Despite their importance, global forest cover has substantially declined in recent decades and, while the rate of net forest loss has recently slowed (FAO, 2024) these ecosystems remain under threat from diverse land-use drivers and environmental pressures. Globally, approximately 27 % of forest loss is directly attributed to permanent land-use change for commodity production (*e.g.*, beef, soy, palm oil, and wood fiber) (Curtis et al., 2018). The remaining loss is driven by other land-use dynamics, alongside compounding climate-related stressors such as mega-fires, biotic outbreaks, and prolonged droughts (McDowell et al., 2020; Seidl et al., 2017). As these pressures reduce the carbon sink capacity of forests, altering atmospheric greenhouse gas concentrations (Houghton and Nassikas, 2017; IPCC, 2023), accurate estimation of forest aboveground biomass (AGB) has become increasingly essential for informing climate mitigation strategies (Houghton et al., 2009; IPCC, 2019). Such estimates are critical for monitoring carbon budgets and fluxes at global and national scales and are fundamental to greenhouse gas inventories and mitigation commitments, including Nationally Determined Contributions (NDCs) under the UNFCCC and Paris Agreement frameworks (Friedlingstein et al., 2025).

The geographic distribution of forest biomass stocks is controlled by complex interactions between forest structure and ecological processes (Pan et al., 2013). These dynamics depend on multiple factors, including climate, soil properties, and the growth rate of dominant tree species, as well as the frequency and intensity of both natural and anthropogenic disturbances (Keith et al., 2009). Central to understanding the role of forests as carbon sinks is the balance between biomass gain and loss (Pan et al., 2013). When this equilibrium shifts toward net loss, the capacity for carbon sequestration decreases, potentially transforming forests into net sources of greenhouse gas emissions. Estimating forest carbon loss remains a major global challenge, with considerable uncertainty arising from the spatial variability of forest carbon stocks (Harris et al., 2021). This challenge is particularly acute for native forests. Robust landscape-scale carbon estimates critically depend on high-quality field data, which are often scarce for non-commercial native species because historical forest inventories largely prioritized volume estimations for commercially valuable timber (Picard et al., 2012).

In Chile, native forests cover approximately 20.5 % of the national territory, distributed between ~32° S and 56° S (CONAF, 2025). Some of these forests are recognized as biodiversity hotspots due to their high levels of plant endemism (Mittermeier et al., 2004; Myers et al., 2000). These ecosystems include the southernmost forests on the planet, located in subantarctic Patagonia (Miranda et al., 2023). Structurally, Chile's native forests are highly diverse, including stunted, intermediate, secondary, and primary forests, which account for approximately 19 %, 16 %, 31 %, and 34 % of the total native forest area, respectively (CONAF, 2025). This broad structural and ecological variability, ranging from semi-arid Mediterranean shrublands to ancient temperate rainforests, makes these ecosystems relevant at both national and global

https://doi.org/10.5194/essd-2026-720
Preprint. Discussion started: 9 November 2026
© Author(s) 2026. CC BY 4.0 License.



scales. Nationally, native forests represent the only net carbon sink in Chile's National Greenhouse Gas Inventory (Basoa et al., 2024; Gómez-González et al., 2024) and globally they constitute important carbon reservoirs containing extensive Intact Forest Landscapes and irrecoverable carbon stocks (Noon et al., 2021).

Quantifying native forest biomass in Chile is challenging due to its high structural diversity and the logistical constraints associated with the remote location of many of these ecosystems. Moreover, forest data in Chile have been collected for varying research objectives and with differing levels of precision. Consequently, the absence of a uniform national database introduces considerable uncertainty into forest cover statistics and biomass density estimates at the national scale (Altamirano et al., 2015). This issue is exacerbated by the ongoing degradation of native forests caused by cattle grazing, selective logging, and wildfires, processes that have been underestimated and that directly affect the structural conditions and carbon stocks of these ecosystems. This, in turn, limits the ability to generate reliable national baseline figures, which are essential for developing effective climate change mitigation policies based on forests' carbon sink capacity (González et al., 2026). Generating open, accessible, and spatially explicit data is therefore essential for characterizing Chile's carbon reservoirs, informing forest planning and management, and fulfilling international climate change mitigation commitments that depend on accurate carbon stock estimates (Milla et al., 2013).

The Chilean Forest Service (Corporación Nacional Forestal, CONAF) has long monitored national forest cover, providing freely available data (CONAF, 2025). For example, CONAF's National Forest Biomass and Carbon Monitoring Project established an extensive network of permanent field plots across ecoregions with distinct biogeographic and bioclimatic profiles, covering a latitudinal range of approximately 2,800 km from 30° to 56° S (CONAF, 2015). However, a harmonized, open-access forest biomass and carbon database remains unavailable.

Here, we present a large-scale or measurements and plot-level estimates of living-tree biomass and carbon stocks in Chilean native forests. The resource integrates 59,408 tree records from 2,024 field plots, covering 77 species, 12 Chilean forest types and approximately 2,800 km of latitude. Biomass estimates were derived using nationally applicable allometric equations, complemented by model-assisted estimates for individuals outside their assigned calibration ranges, particularly addressing large-diameter or uncommon tree species. The data are additionally harmonized by forest stand development and Plant Functional Type (PFT), facilitating use across national and international forest-monitoring frameworks. This represents the first large-scale, open-access biomass and carbon density dataset for Chile's national forest inventory.

2. Materials and methods

2.1 Study area

The study area extends from the Coquimbo Region (29° S) to the Magallanes Region (56° S) (Fig. 1). Across the study area, the complex topography, shaped by the Coastal Range and the Andes Mountains, generates an altitudinal gradient from sea level to over 5,000 m a.s.l. (Fig. 2a). This gradient, in interaction with latitude, strongly influences vegetation distribution, forest structure, and composition (Donoso, 2013). Within this latitudinal range, 99 % of the country's native forests are located (Fig. 1), covering approximately 15.4 Mha (CONAF, 2025).

https://doi.org/10.5194/essd-2026-720
Preprint. Discussion started: 9 November 2026
© Author(s) 2026. CC BY 4.0 License.

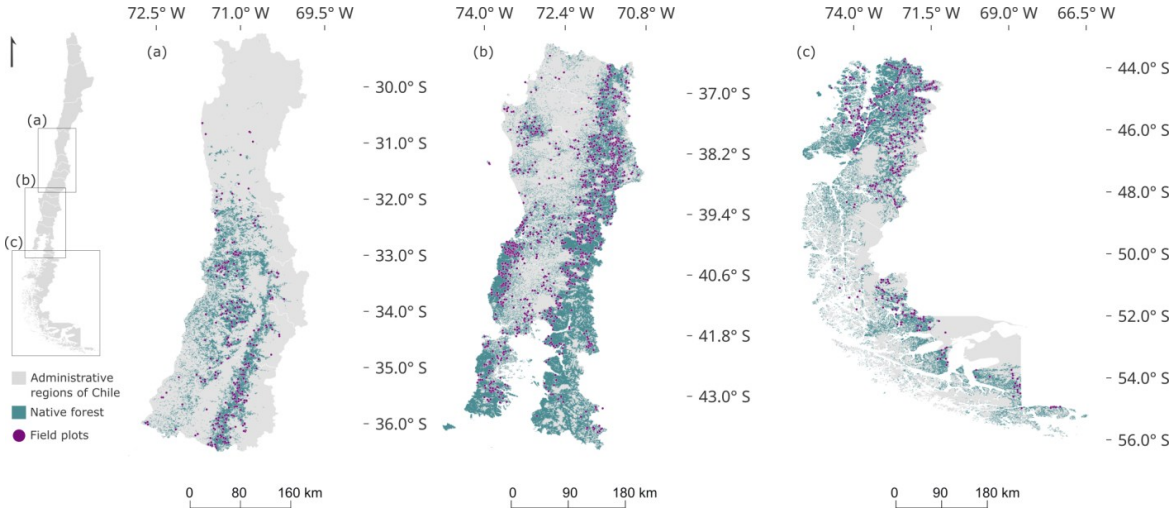


Figure 1. Geographic distribution of native forests and field plots measured under the *National Forest Biomass and Carbon Monitoring Project in Chile*. The central and southern part of the country was divided into three zones bounded by administrative regions: (a) Coquimbo to Maule (29.5° to 36.5° S); (b) Ñuble to Los Lagos (36.5° to 44° S) including three field plots outside the continental territory at ~ 38.2° S (Mocha island); and (c) Aysén and Magallanes (44° to 56° S). The native forest cover map was obtained from CONAF (2025).

Biogeographically, field plots span from the isolated relict forests of Fray Jorge (30.3° S) and drought-adapted sclerophyllous forests of the northern and central Mediterranean climate zones to species-rich broadleaf evergreen temperate forests in the south, and subantarctic ecosystems in the extreme south. Latitudinal compensation strongly mediates the elevational distribution of these ecosystems, with forest types occurring at high elevations in the central and northern Andes shifting progressively to sea level in the southernmost latitudes as temperatures decrease (Donoso et al., 2014). Structured by the combined latitudinal and altitudinal gradients and based primarily on dominant species associations, these forests have been categorized into 12 Chilean forest types for national management and conservation purposes (Donoso, 1981) (Fig. 2b). In a broader ecological context, these forest types span across distinct ecoregions (Fig. 2c), including the Chilean matorral, Valdivian temperate forests, and Magellanic subpolar forests (Dinerstein et al., 2017), the last of which is referred to as Magellanic subantarctic forests for consistency with local literature.

https://doi.org/10.5194/essd-2026-720
Preprint. Discussion started: 9 November 2026
© Author(s) 2026. CC BY 4.0 License.

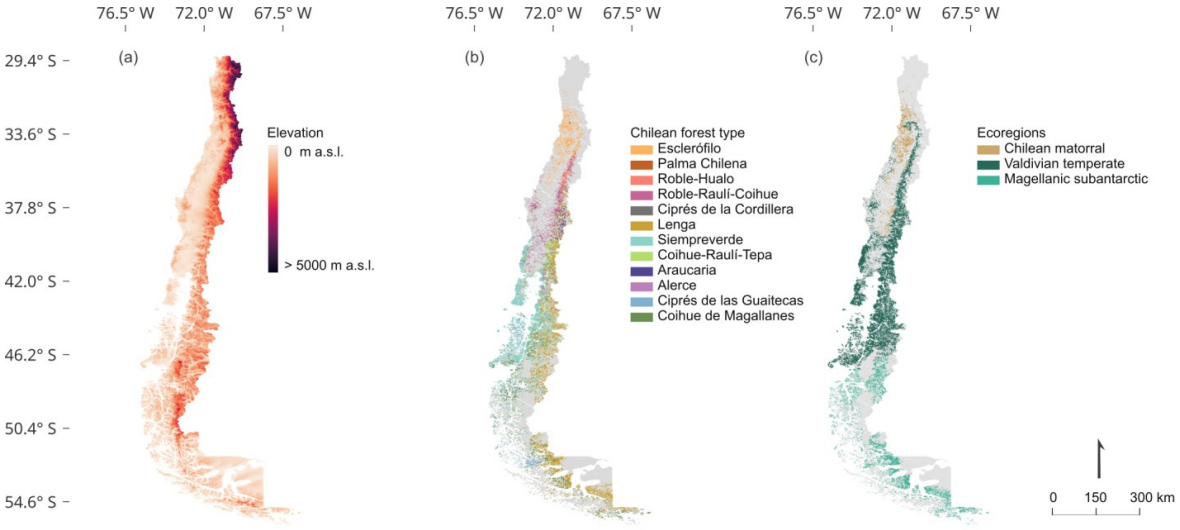


Figure 2. Study area: (a) Elevation above sea level (m a.s.l.) (European Space Agency, 2024); (b) Geographical distribution of Chilean forest types (Donoso, 1981); and (c) ecoregions classification (Dinerstein et al., 2017).

2.2 Data and processing

2.2.1 Field data

We used data from 2,024 field plots located between the Coquimbo (29.5° S) and Magallanes (56° S) administrative regions, obtained by CONAF under the *National Forest Biomass and Carbon Monitoring Project* between 2011 and 2020 (Fig. 1). Measurement year is retained for each plot, allowing users to account for the temporal distribution of the inventory. Data collection followed standardized protocols from CONAF's Field Operations Manual (CONAF, 2015). Each field plot covered 500 m^2 (10 × 50 m). This sampling design effectively captures the localized structural patchiness and the fine-scale mosaic of disturbance and recovery phases inherent to primary forests. Field work recorded tree-level parameters included: i) species, ii) diameter at breast height (DBH), iii) diameter at stump height (DSH), and iv) total height (H). Plot-level attributes comprised Chilean forest type, forest stand development, and ecoregion.

To facilitate global comparisons and alignment with international reporting standards, the 12 Chilean forest types were also classified into three broader PFTs based on leaf habit: broadleaf deciduous, broadleaf evergreen, and needle-leaf evergreen. For Chilean forest types (e.g., *Roble-Raulí-Coihue* and *Coihue-Raulí-Tepa*), PFT assignment was determined by the Chilean forest subtype, which describes the dominant species composition within each plot. For example, plots within the *Roble-Raulí-Coihue* type were classified as broadleaf evergreen if the subtype was dominated by the evergreen *Nothofagus dombeyi*, but as broadleaf deciduous if the subtype was dominated by the deciduous *Nothofagus obliqua*. PFT assignments for all Chilean forest types and subtypes are provided in Supplementary material (Table A1).

In total, the inventory dataset encompasses 59,408 individual tree measurements. Broadleaf evergreen species represent the dominant component of the sampled forests, harboring the highest tree abundance, species richness and diversity (Table 1). Structurally, mean diameter (DBH) and mean total height (H) remain relatively consistent across all three PFTs.

https://doi.org/10.5194/essd-2026-720
Preprint. Discussion started: 9 November 2026
© Author(s) 2026. CC BY 4.0 License.



143 However, clear structural and compositional gradients emerge at the ecoregion level. The Valdivian temperate ecoregion
144 drives the overall dataset trends, accounting for over 80 % of the measured trees and exhibiting the highest structural
145 dimensions and species diversity. In contrast, the Chilean matorral ecoregion reflects environmental constraints showing
146 markedly lower mean DBH and height. Conversely, a latitudinal diversity gradient is evident in the southernmost Magellanic
147 subantarctic forests; while these forests maintain structural dimensions comparable to the Valdivian temperate ecoregion,
148 they exhibit a pronounced reduction in species richness and evenness.

Table 1. Tree-level metrics grouped by PFTs and ecoregions.

Group	n of trees	BA (m^2 ha^{-1}) ± SD	DBH (cm)	H (m)	SR	SH	Evenness
Plant functional type							
Broad leaf deciduous	19202	1.3 ± 2.4	22.8	11.6	54	2.3	0.6
Broad leaf evergreen	34812	1.5 ± 4.1	22.9	12.5	73	3.4	0.8
Needle leaf evergreen	5394	1.4 ± 2.6	23.1	11	41	2.9	0.8
Ecoregion							
Chilean matorral	3723	0.5 ± 1	12.6	8.3	49	2.8	0.72
Valdivian temperate	48212	1.5 ± 3.8	23.6	12.5	75	3.4	0.78
Magellanic subantarctic	7473	1.2 ± 1.8	23.4	11.5	20	1.7	0.56

Note: BA = Basal area; SD = Standard deviation of BA; DBH = Diameter at breast height; H = Total height; SR = Species richness; SH = Shannon diversity index. All metrics represent the mean value for the groups.

149

150 The resulting inventory contains 59,408 individual-tree records from 2,024 plots and 77 species, constituting the core
151 observational resource of the dataset. Forest stand development was classified based on definitions from CONAF's Field
152 Operations Manual (CONAF, 2015) (Fig. 3). CONAF defined four forest stand development based on structural complexity:
153 i) primary, ii) intermediate, iii) secondary, and iv) stunted forests. Primary forests are defined as late-successional, mature
154 stands characterized by high structural heterogeneity, including complex vertical stratification, variable crown sizes, and a
155 wide distribution of tree diameters and ages. Intermediate forests are defined as transitional stands comprising a mixture
156 of mature canopy trees and younger regenerating cohorts, representing mixed-aged phases where primary and secondary
157 structures coexist. Secondary forests are defined as young, early-to-mid successional forests that originated via seed or
158 vegetative reproduction following a natural or anthropogenic stand-replacing disturbance. In contrast to primary forests,
159 these stands typically exhibit a more homogeneous vertical structure and diameter distribution. Stunted forests are
160 defined as stands whose structure is primarily determined by severe environmental constraints. These are subdivided into
161 tall stunted forests, which are typically primary stands that maintain a homogeneous physiognomy similar to secondary
162 forests due to site restrictions, and low stunted forests, which reach approximately 2 m in height and are characterized by
163 multi-stemmed growth forms in response to extreme abiotic stress, including freezing temperatures and strong winds.

164 The sampling design within each field plot was defined based on ecoregion and forest stand development. For the Valdivian
165 temperate and Magellanic subantarctic ecoregions, primary and intermediate forests followed a full-plot design, in which
166 all individuals with DBH ≥ 10 cm and H ≥ 2 m were measured across the entire 500 m^2 area (Fig. 3a). Secondary forests
167 used a nested subplot design, in which large trees (DBH ≥ 30 cm) were measured across the full 500 m^2 plot, while smaller
168 trees (10 cm ≤ DBH < 30 cm) were measured only within a 250 m^2 subplot, with H ≥ 2 m required in both cases (Fig. 3b).

https://doi.org/10.5194/essd-2026-720
Preprint. Discussion started: 9 November 2026
© Author(s) 2026. CC BY 4.0 License.

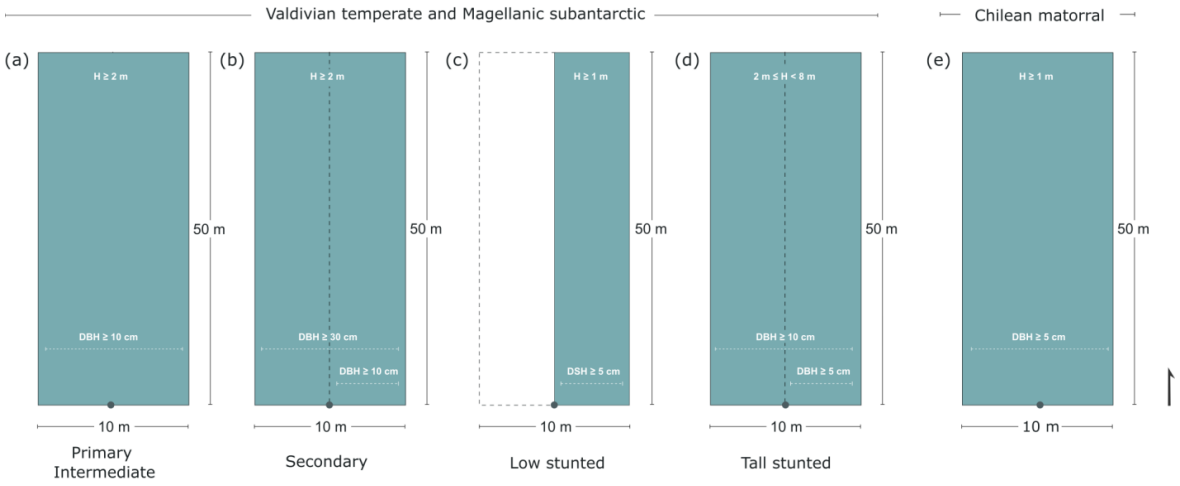


Figure 3. Field plot designs following CONAF (2015) for: (a) primary and intermediate forest, (b) secondary forest, (c) low stunted forest, and (d) tall stunted forests in the Valdivian temperate, and Magellanic subantarctic ecoregions; and (e) the Chilean matorral.

For stunted forests within the southern ecoregions, the field plot design was defined based on canopy height. Low stunted forests were measured in a 250 m^2 subplot for all individuals with a DSH ≥ 5 cm and H ≥ 1 m (Fig. 3c). In contrast, tall stunted forests followed a nested design where trees with DBH ≥ 10 cm were recorded across the full 500 m^2 plot, and smaller trees (5 cm ≤ DBH < 10 cm) were recorded in a 250 m^2 subplot, with measurements restricted to individuals with 2 m ≤ H < 8 m (Fig. 3d). Finally, for the Chilean matorral ecoregion, a uniform design was applied across all forest stand development (Fig. 3e), in which all individuals with DBH ≥ 5 cm and H ≥ 1 m were measured across the entire 500 m^2 plot. Tree height was measured on a subsample of at least 10 trees per field plot, regardless of ecoregion or forest stand development. These trees were selected to represent the various diameter classes present, ensuring at least three height measurements per species. The sampling design defined the expansion factors required to scale tree-level measurements to area-based densities (Mg ha^{-1}) (Fig. 3, Table 2).

Table 2. Field plot sampling criteria and expansion factors used to scale tree-level aboveground biomass (AGB, Mg) to plot-level aboveground biomass density (AGBd, Mg ha^{-1}).

Ecoregion	Stand development[a]	DBH[b] (cm)	DSH[b] (cm)	Area (m^2)	Expansion factor
Valdivian temperate and Magellanic subantarctic	Primary forest Intermediate forests	≥ 10	-	500	20
	Secondary forest	≥ 30		500	20
		$\geq 10\ and < 30$	-	250	40
	Low stunted	-	≥ 5	250	40
	Tall stunted	≥ 10	-	500	20
		$\geq 5\ and\ < 10$	-	250	40
Chilean matorral	-	≥ 5	-	500	20

https://doi.org/10.5194/essd-2026-720
Preprint. Discussion started: 9 November 2026
© Author(s) 2026. CC BY 4.0 License.



Open Access Earth System Science Data Discussions

[a]Forest structure, forest stand development, and inclusion criteria follow the standardized protocols from CONAF's *Field Operations Manual* (CONAF, 2015).

[b]DBH = diameter at breast height; DSH = diameter at stump height.

2.2.2 Height estimations

To address missing H records required for individual carbon stock estimation, we developed a predictive height-diameter model. We employed linear mixed-effects models (LME) using the *nlme* package in R (Pinheiro et al., 2023). This framework accounts for the hierarchical nature of forest data, where individual trees are nested within plots and species. By specifying these levels as random effects, the models account for the non-independence of observations from the same spatial location and taxon. This approach prevents pseudoreplication and avoids inferential errors that arise from treating clustered forest data as independent observations (Mehtätalo et al., 2015). The height-diameter relationships followed the functional form shown in Eq. (1):

$$H = \beta_0 + \frac{\beta_1}{D} + \beta_2 D + \beta_3 D^2 \quad (1)$$

Where H is the estimated height (m) and D is the tree diameter (cm). DBH was used as the primary predictor, with DSH used as a substitute only when DBH measurements were unavailable. To ensure a complete and robust dataset, we implemented a hierarchical fallback strategy to predict heights for individuals lacking field measurements. The models (Eq. (1)) were applied in descending order of taxonomic and spatial levels:

- Level 1: Predictions were derived from a model using DBH with a nested random-intercept structure: species nested within plots.
- Level 2: For individuals for which the species–plot combination lacked sufficient observations to support the nested model, a model using DBH with species as a global random intercept was applied.
- Level 3: In the absence of DBH measurements, the procedure was repeated using DSH as the primary predictor, following the same hierarchical order.
- Level 4: For uncommon tree species, generalized models based on DSH and plot-level random effects were used.

These tree-level predictions ensured a biologically plausible height profile for the dataset (Table A2 in Appendices), capturing both site-specific and taxonomic variability.

2.2.3 Biomass and carbon estimation

Tree-level aboveground biomass (AGB) was estimated using published allometric equations, successfully covering nearly all tree species (98.7 %) recorded in the field plots (the full list of equations and sources is provided in the Data availability section). We prioritized species-specific models; when these were unavailable, equations from species with similar taxonomic or ecological characteristics were applied as proxies. The number of utilized equations exceeds the number of species because we accounted for geographical variation. Specifically, when multiple equations were available for a widely distributed species, the appropriate model was assigned based on the plot's latitude, longitude, and altitude. This approach ensured that AGB estimates accurately reflected site-specific environmental conditions across the extensive

https://doi.org/10.5194/essd-2026-720
Preprint. Discussion started: 9 November 2026
© Author(s) 2026. CC BY 4.0 License.



latitudinal gradient of the study area. Regarding the model structures, 63 % of the compiled equations required both DBH and H for biomass calculation, while 30 % used only DBH, and 7 % relied solely on DSH.

Approximately 29 % of trees fell outside the DBH or H calibration ranges of their assigned allometric equations. Since applying equations directly beyond their calibration domains could lead to large errors in the estimations, biomass for these individuals was estimated using a Boosted Regression Trees (BRT) predictive model to fill these estimation gaps and provide biomass estimates for those individuals for which the available allometric equations could not be applied reliably. This model-assisted approach allowed biomass to be estimated for all trees in the inventory while accommodating nonlinear relationships among DBH, height, species, forest type and stand development, particularly for uncommon or large-diameter individuals. The approach is based on Generalized Gradient Boosting Machines (Friedman, 2001), which was selected for its ability to handle non-linear relationships and high-order interactions without the constraints of linear, power, or polynomial regressions.

The BRT model was formulated to predict the natural logarithm of biomass using five predictor variables: DBH, H, species, Chilean forest type, and forest stand development. The BRT model estimated the final prediction as a weighted, additive sum of individual regression trees, initialized at the mean value of log-transformed biomass. The model followed the functional form shown in Eq. (2):

$$\ln(B) = f_0(\boldsymbol{x}) + \sum_{m=1}^{M} \eta \cdot T_m(\boldsymbol{x}; \theta_m) \quad (2)$$

Where ln(*B*) is the predicted natural logarithm of biomass (*B*, in kg), $\boldsymbol{x}$ represents the vector of the five dendrometric and categorical predictors, f_0 is the initial constant, *M* is the total number of individual trees in the ensemble, η is the learning rate, and T_m represents the m-th individual tree with parameters θ_m.

The model was implemented using the *gbm* and *dismo* packages in R (Hijmans et al., 2023; Ridgeway et al., 2003). The *gbm.step* function was used for model tuning and selection of the optimal *M* via ten-fold cross-validation. A Gaussian loss function was used for fitting. The hyperparameters were set to optimize generalizability: learning rate (η) = 0.01; tree complexity (θ_m) = 3, and bag fraction = 0.5. To ensure a robust assessment of the model's predictive power, the dataset was partitioned: 80 % (n = 33,852) for training and 20 % (n = 8,464) for independent validation. Evaluation metrics, including Root Mean Square Error (RMSE), Mean Absolute Error (MAE) and coefficient of determination (R^2), were calculated on the on the held-out validation set.

Due to the nested sampling design, individual tree-level AGB was first scaled to aboveground biomass density (AGBd, Mg ha^{-1}) by applying the corresponding expansion factor (Table 2). This factor was determined by the tree's dimensions and the subplot area in which it was measured. Scaling at the individual tree level was necessary to account for the different sampling thresholds within a single plot.

The conversion of AGBd to aboveground carbon density (AGCd, MgC ha^{-1}) was conducted following the region-specific guidelines established by Gayoso and Guerra (2005):

https://doi.org/10.5194/essd-2026-720
Preprint. Discussion started: 9 November 2026
© Author(s) 2026. CC BY 4.0 License.



a) Species-specific tissue approach: For species with detailed data available, AGCd was calculated at the tissue level (stem, branches, leaves, and bark). Total tree AGBd was first partitioned into these compartments using the empirical biomass distribution percentages reported by (Gayoso et al., 2002). Subsequently, compartment-specific carbon concentrations were applied using the factors determined by (Gayoso and Guerra, 2005). Total tree carbon was calculated as the sum of the carbon content across all tissues (Eq. (3)):

$$C_{total} = \sum_{i=1}^{n} (B_i \times CF_i) \quad (3)$$

Where B_i is the biomass density of tissue i, and CF_i is the corresponding carbon fraction for that tissue.

b) General conversion approach: For species without specific tissue data, a carbon conversion factor of 0.4964 was applied directly to the total tree AGBd. This value corresponds to the weighted average recommended by Gayoso and Guerra (2005) for non-specified Chilean native species.

Following these tree-level calculations, AGCd values were aggregated within each plot to yield the total aboveground carbon density per plot. Finally, differences in AGBd across forest stand development, within each PFT and ecoregion, were evaluated using non-parametric Kruskal-Wallis tests, using *rstatix* packages (Kassambara, 2019) (reporting the *H* statistic and *p*-value in Table A3 and A4).

Recognizing quantitative uncertainty as a fundamental requirement for large-scale carbon assessments (Chave et al., 2004), an error propagation framework was implemented using a Monte Carlo simulation approach (n=1,000 iterations) (Holdaway et al., 2014; Li et al., 2022). The propagated plot-level uncertainty considered the relative contribution of species-specific allometric estimates and BRT-assisted estimates. For individuals with direct allometry, the residual standard error (RSE) of the respective published equations was incorporated into the simulation. For trees lacking specific allometries, the Root Mean Square Error (RMSE) of the BRT model was integrated to propagate model prediction uncertainty (Li et al., 2022). Furthermore, uncertainties related to carbon fraction conversions were included (Gayoso and Guerra, 2005). Through these stochastic iterations, the standard error (SE) and 95 % confidence intervals were generated for each plot. The resulting intervals therefore represent the uncertainty components explicitly propagated in the analysis rather than complete inventory uncertainty.

3 Results and discussion

To generate the plot level database, we use directly measured living trees, representing 77 species across the Chilean forest types. When grouped by Plant Functional Type (PFT), broadleaf evergreens accounted for 59 %, followed by broadleaf deciduous (32 %) and needle-leaf evergreens (9 %). These individuals were relatively evenly distributed across forest stand development, with 31.2 % recorded in primary forests, 31.1 % in intermediate forests, and 37.7 % in secondary forests. Tree DBH ranged from 5 to 530 cm, reflecting the broad structural diversity of the sampled forests.

https://doi.org/10.5194/essd-2026-720
Preprint. Discussion started: 9 November 2026
© Author(s) 2026. CC BY 4.0 License.



3.1 Tree-level aboveground biomass

The BRT model demonstrated high predictive performance, explaining 97.9 % of the variability in the log-transformed biomass (Fig. 4a). As expected from the geometric scaling of trees, DBH was the most influential predictor (70.1 % relative contribution), followed by species (18.1 %) and total height (11.2 %) (Fig. 4b).

While the model showed high precision in log-space (RMSE = 0.2; MAE = 0.12), these errors increased when back-transformed to absolute biomass (kg), particularly for larger individuals in the validation set. This trend is a common feature in forest allometry, where structural variability, driven by crown architecture and stem defects, becomes more pronounced as trees increase in size (Chave et al., 2014; Jucker et al., 2017). In total, BRT-based estimates were generated for 17,092 of the surveyed trees.

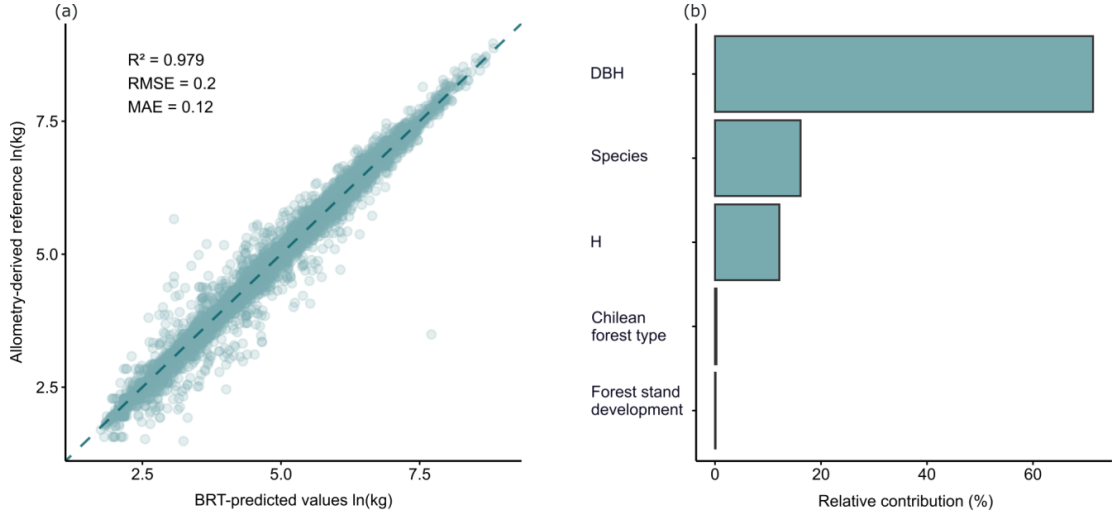


Figure 4. BRT model evaluation for tree-level aboveground biomass (AGB) estimation. (a) Predictive performance of the model on the independent validation set, where the dashed line indicates perfect agreement (1:1) between observed and predicted values in natural logarithmic scale. (b) Relative contribution (%) of the five predictor variables used in the model.

Across all ecoregions, the tree-level biomass distributions exhibited a marked positive skewness (Fig. 5). This frequency pattern is characteristic of natural, uneven-aged forest populations, where a high abundance of small trees coexists with a progressively lower density of larger individuals (Enquist et al., 1999). Globally, this pattern is driven by the internal dynamics of natural forests, where only a small fraction of individuals overcome competitive and environmental constraints to reach exceptionally large sizes (Lutz et al., 2018). In Chile, this pattern reflects the demography of native ecosystems, where continuous recruitment of young trees is balanced by the rare but notable persistence of emergent, long-lived individuals that accumulate substantial biomass over centuries (Lara et al., 2014).

https://doi.org/10.5194/essd-2026-720
Preprint. Discussion started: 9 November 2026
© Author(s) 2026. CC BY 4.0 License.

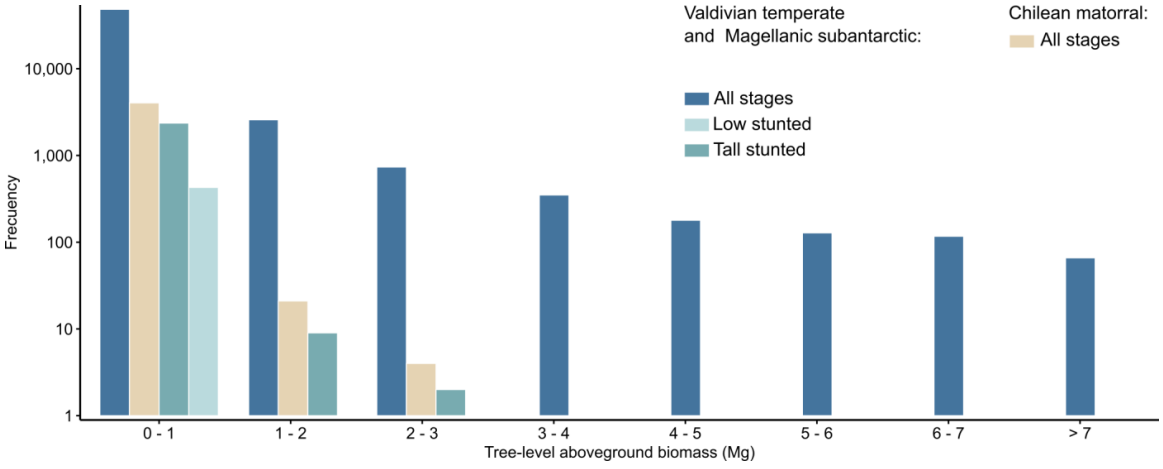


Figure 5. Frequency distribution of tree-level aboveground biomass across the different ecoregions and forest stand development. The frequency (y-axis) is displayed on a logarithmic scale (log_{10}). Note that the Chilean matorral is represented as a single aggregated category encompassing all forest stand development, reflecting its uniform field sampling design across the ecoregion.

The Valdivian temperate and Magellanic subantarctic ecoregions exhibited both the greatest number of observations (n = 55,685), with multiple individuals exceeding 7 Mg (Fig. 5). These high values are consistent with the dimensions of emergent trees occurring in primary forests of southern Chile, such as the broadleaf evergreen *Nothofagus dombeyi*, the subantarctic *Nothofagus betuloides*, the conifer *Fitzroya cupressoides*, and *Araucaria araucana*, all species capable of accumulating substantial biomass over centuries (Aguilera-Betti et al., 2017; Soto et al., 2010; Urrutia-Jalabert et al., 2015). These southern ecoregions contained the highest individual-tree biomass values represented in the dataset, aligning with global assessments that highlight the exceptional carbon storage potential of temperate rainforests (Keith et al., 2009; Luyssaert et al., 2008; Schlegel, 2001).

In contrast, the Chilean matorral ecoregion exhibited a skewed distribution but within a far more restricted range, where most individuals fell below 1 Mg and only a few reached 2-3 Mg (Fig. 5). This ecoregion is dominated by sclerophyllous species whose biomass accumulation is physiologically constrained by the prolonged summer droughts characteristic of Mediterranean-type climates (Sardans and Peñuelas, 2013; Veblen et al., 2007). Within this community, a trade-off between abundance and individual size is evident: while widely distributed species like *Cryptocarya alba* and *Lithraea caustica* typically maintain relatively small aboveground biomass, the upper biomass range is represented by scarcer species such as *Quillaja saponaria*, *Jubaea chilensis*, or *Beilschmiedia miersii*, which can exceed 2.5 Mg (Hurtado, 2012; Milla et al., 2013). Centuries of intense land-use change and native forest loss in central Chile have disproportionately eliminated these larger legacy trees, leaving a landscape dominated by small, young, or resprouting individuals (Miranda et al., 2017).

Finally, stunted forests (encompassing both low and tall structural forms) exhibited the constrained individual biomass development, with individuals rarely exceeding 3 Mg (Fig. 5). This structural limitation is a permanent physiognomic adaptation to extreme abiotic stressors typical of high-latitude or treeline environments, such as chronic wind exposure, cryogenic soil processes, and a short growing season (Piper et al., 2016). This pattern is consistent with the high phenotypic

https://doi.org/10.5194/essd-2026-720
Preprint. Discussion started: 9 November 2026
© Author(s) 2026. CC BY 4.0 License.



plasticity of dominant species like *Nothofagus pumilio*, which adjusts its growth form in response to environmental constraints that impose a metabolic ceiling on individual development. Consequently, these trees remain small even at maturity, resulting in ecosystems characterized by high stem density but low individual biomass, consistent with patterns of temperature-driven growth limitation (Fajardo and Piper, 2011; Körner, 2012; Lara et al., 2014).

3.2 Plot-level aboveground biomass density

The stratification of plots by PFTs and forest stand development revealed high heterogeneity in plot-level AGBd estimates (Fig. 6a; Table A3 in Appendices). A consistent pattern among stand-development classes was evident across PFTs, with mean AGBd decreasing from primary to intermediate and secondary forests. These differences in biomass across forest stand development were highly significant for all functional types (Kruskal-Wallis tests, all $p < 0.01$; broadleaf deciduous: $H = 85.15$; broadleaf evergreen: $H = 223.45$; needleleaf evergreen: $H = 30.22$). While data dispersion decreased with stand age in broadleaf ecosystems, intermediate stands of needleleaf evergreens exhibited an even wider interquartile range than primary forests. Primary forests, late-successional ecosystems with complex vertical structure and emergent individuals, consistently showed the highest mean AGBd across all PFTs compared to younger stands (Franklin et al., 2002).

Within the broadleaf evergreen group (Fig. 6a), mature rainforests (*e.g.*, *Siempreverde* Chilean forest type) exhibited large carbon-storing potential, with primary forests averaging 291 Mg ha^{-1}, with extreme values surpassing 700 Mg ha^{-1}. However, this PFT also encompasses environmentally constrained ecosystems subjected to Mediterranean climates with marked summer droughts. Sclerophyllous woodlands within this PFT exhibited markedly lower AGBd means (consistently below 50 Mg ha^{-1} in the *Esclerófilo* Chilean forest type; Table A5 in Appendices), which largely explains the exceptionally wide interquartile range and data dispersion observed in this overarching category.

Similarly, large standing stocks were observed in broadleaf deciduous group (Fig. 6a) dominated by *Nothofagus* species (*e.g.*, *Lenga* and *Roble-Raulí-Coihue* Chilean forest type; Table A5 in Appendices) where primary forests concentrated the highest means (266 Mg ha^{-1}) and largest data ranges, progressively constricting towards secondary stages (127 Mg ha^{-1}).

The forest of needle-leaf evergreen (Fig. 6a), composed of long-lived conifers, also demonstrated high AGBd means in primary forests (235 Mg ha $^{-1}$) and intermediate development stages (218 Mg ha $^{-1}$), with individual plot estimates approaching 800 Mg ha $^{-1}$. This reflects the high heterogeneity of these mixed-aged phases where legacy trees coexist with younger cohorts. These standing stocks are heavily dependent on the presence of large-diameter individuals, as a small subset of the largest trees in a stand typically accounts for nearly half of the total live biomass in mature forests (Lutz et al., 2018). Conversely, needle-leaf ecosystems, specifically those dominated by Chilean forest types as *Ciprés de la Cordillera* and *Ciprés de las Guaitecas* exhibited constrained biomass ranges and low mean values (< 200 Mg ha^{-1}).

Across these highly productive primary and intermediate forests, the large interquartile range and extreme values indicate substantial structural heterogeneity. This sharply contrasts with the narrower distributions seen in secondary stands and environmentally constrained ecosystems, which lack the structural complexity to develop large canopy gaps and emergent trees. This variance in mature, highly productive ecosystems reflects a fundamental ecological pattern where standing biomass is disproportionately concentrated in a few dominant individuals (Slik et al., 2013).

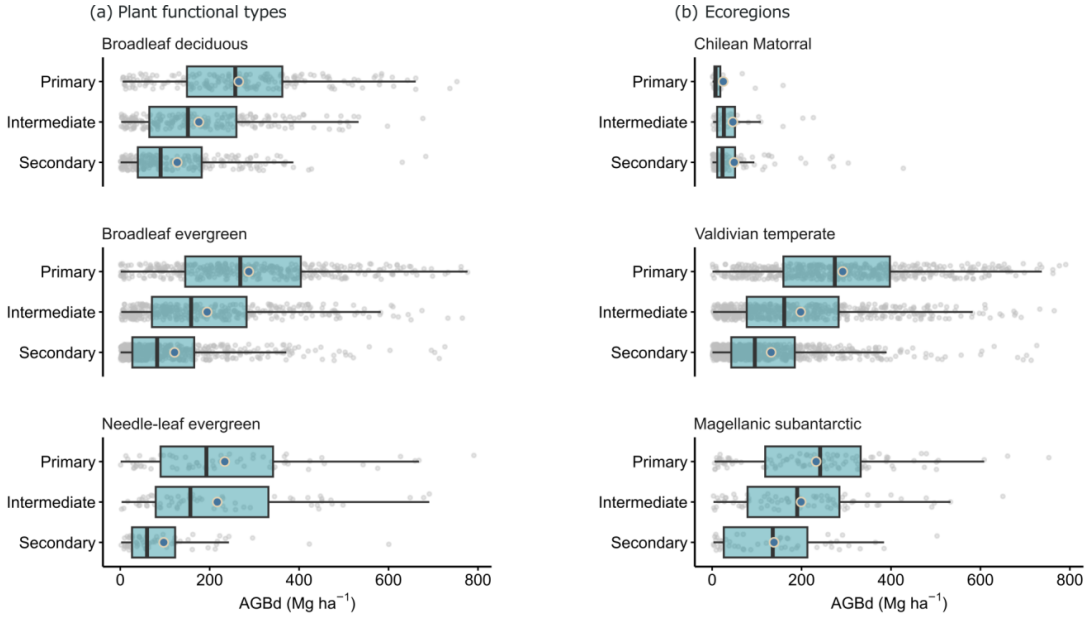
https://doi.org/10.5194/essd-2026-720
Preprint. Discussion started: 9 November 2026
© Author(s) 2026. CC BY 4.0 License.



While PFT reveals trait-based patterns of biomass potential, the actual accumulation of these standing stocks is ultimately limited by large-scale bioclimatic constraints. Ecoregion-level grouping of field plots clearly illustrates this geographic divergence (Fig. 6b; Table A4 in Appendices). This analysis confirmed the Valdivian temperate and Magellanic subantarctic forests as the densest carbon reservoirs, with primary forest AGBd means ranging between approximately 233 and 295 Mg ha^{-1}.

In the highly productive southern ecoregions (*i.e.*, Valdivian temperate and Magellanic subantarctic), a consistent and statistically significant decrease in both mean AGBd and structural variability was observed towards secondary forest (Kruskal-Wallis tests, both $p < 0.01$; Valdivian temperate: $H = 293.77$; Magellanic subantarctic: $H = 13.34$), reflecting the reduced time available for structural diversification and biomass concentration.

In contrast, the Chilean Matorral exhibited a uniquely heterogeneous structural dynamic. Because ecoregions are delineated at a broad geographic scale, the spatial boundary of the Chilean Matorral encompasses more than just purely sclerophyllous vegetation limited by seasonal water deficits (Sardans and Peñuelas, 2013). It also extends into southern transition zones that host denser, higher-biomass Chilean forest types (*e.g.*, *Siempreverde* and *Lenga*). However, primary and intermediate stages within this ecoregion displayed means approaching 25 to 46 Mg ha^{-1}. Specifically, we observed overlaps among forest stand development; several secondary plots exhibited more high biomass levels, while some primary stands ranked low. Due to high internal variability and weak separation between successional stages, the differences in aboveground biomass across stand development stages in the Chilean matorral were weaker than in the southern ecoregions, although the overall difference remained statistically significant ($H = 7.88$, $p < 0.05$) (Table A4 in Appendices). This distribution reflects a complex regional mosaic where arid-limited vegetation is grouped alongside highly productive transitional forests.



https://doi.org/10.5194/essd-2026-720
Preprint. Discussion started: 9 November 2026
© Author(s) 2026. CC BY 4.0 License.



Figure 6. Aboveground biomass density (AGBd) across (a) Plant functional types and (b) Ecoregions, grouped by forest stand development. The blue dot inside each boxplot indicates the mean of AGBd. Scattered gray points represent the individual plot-level estimates to illustrate the underlying data distribution.

3.3 Aboveground carbon stocks

Aboveground carbon density (AGCd) exhibited a synchronized spatial distribution with AGBd (Fig. 7), reaffirming that forest physical structure is the direct determinant of carbon content. The spatial distribution of AGCd reveals the most substantial carbon reservoirs concentrated within the southern mountain ranges, between 39° S and 46° S. In these latitudes, plot-level estimates reach 803.1 Mg ha^{-1} for biomass and 394.7 MgC ha^{-1} for carbon. These values are consistent with field records from primary forests, where large-statured trees drive disproportionate biomass accumulation.

To place these estimates in a broader context, the stocks observed in these southern temperate rainforests rank not only among the highest for South American ecosystems but also stand out on a global scale (González et al., 2022). When evaluating forest structure, our maximum AGBd exceeds the absolute peaks reported for African tropical forests (749 Mg ha^{-1}) (Lewis et al., 2013) and the upper limits of approximately 600 Mg ha^{-1} observed across pantropical scales (Réjou-Méchain et al., 2014). Regarding carbon stocks, our average density in primary temperate forests (134.4 MgC ha^{-1}; Table A4 in Appendices) is comparable to the mean values reported for neotropical forests (140 MgC ha^{-1}), although lower than those of African (183 MgC ha^{-1}) and Asian (197 MgC ha^{-1}) tropical biomes (Sullivan et al., 2017). This quantitative evidence aligns with global assessments demonstrating that intact temperate and subantarctic broadleaf forests can store equivalent or even greater amounts of biomass per hectare than tropical biomes, primarily due to the longevity, wood density, and massive dimensions of their dominant canopy species (Keith et al., 2009).

https://doi.org/10.5194/essd-2026-720
Preprint. Discussion started: 9 November 2026
© Author(s) 2026. CC BY 4.0 License.

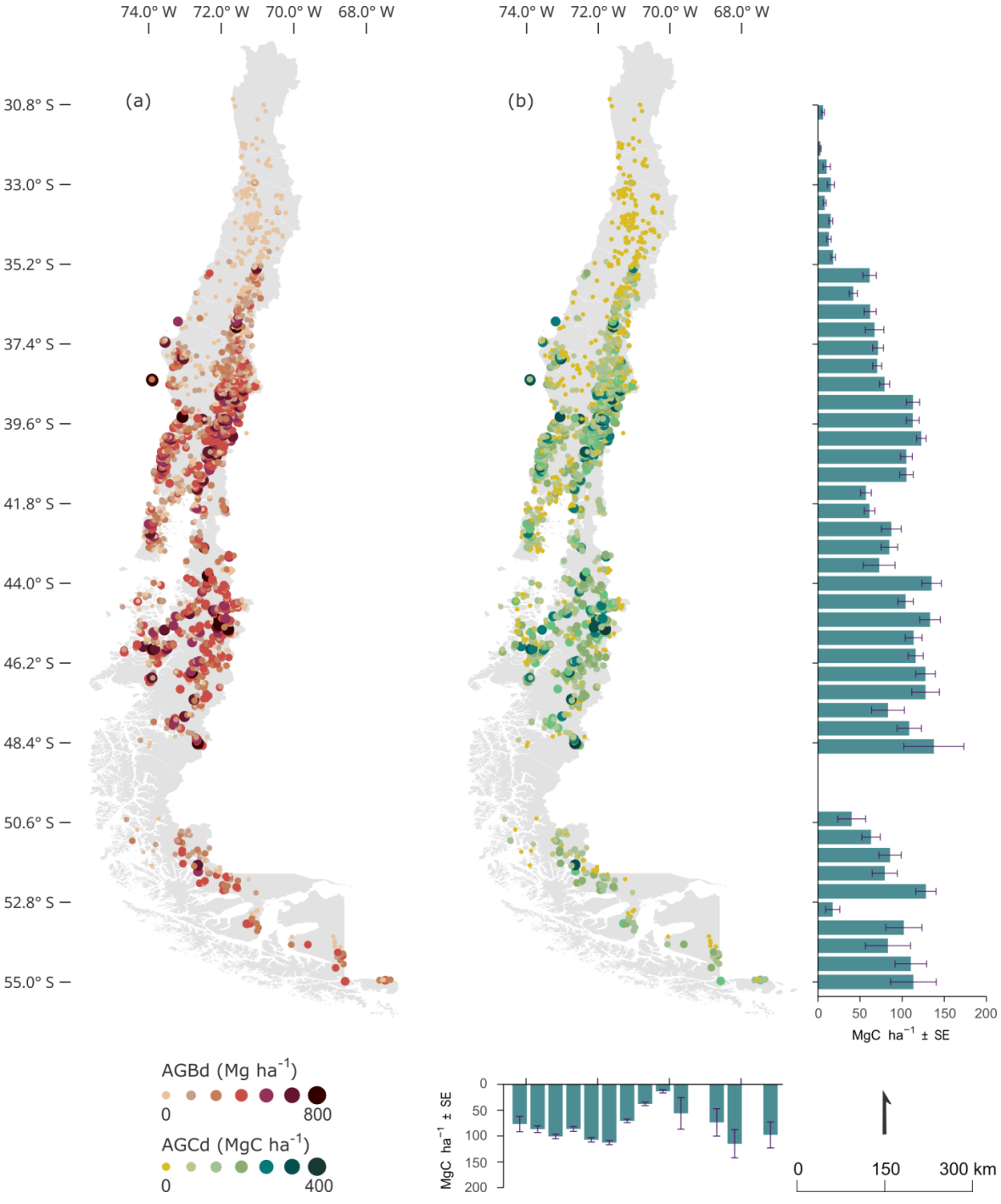


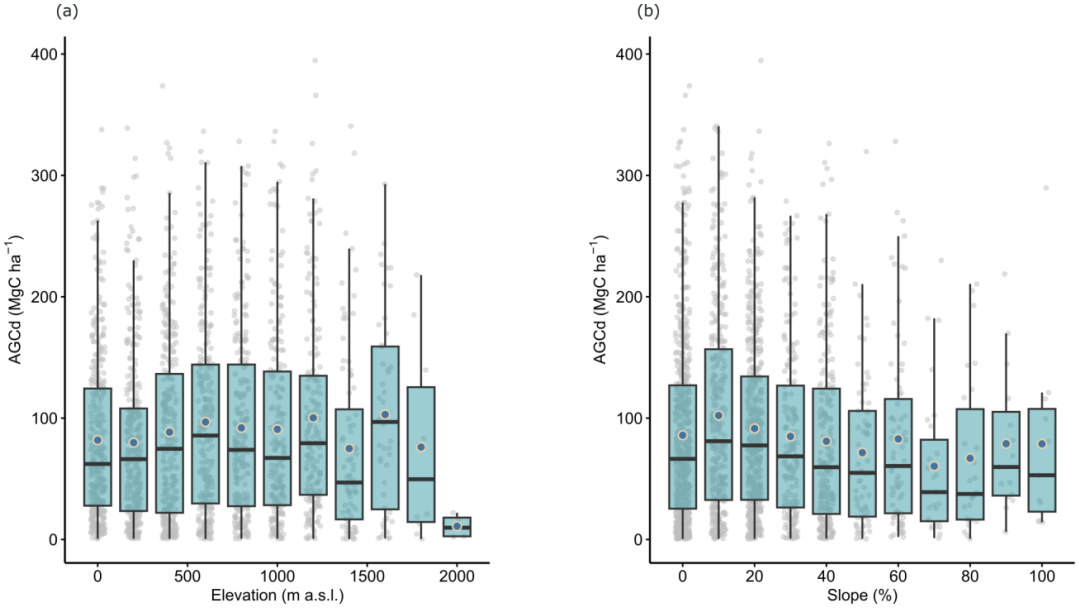
Figure 7. Spatial distribution of (a) aboveground biomass density (AGBd, Mg ha^{-1}) and (b) aboveground carbon density (AGCd, MgC ha^{-1}) in Chile's native forests. Color scales for AGBd and AGCd range from 0 to 800 Mg ha^{-1} and 0 to 400 MgC ha^{-1}, respectively. Marginal bar plots in (b) illustrate the distribution of mean AGCd (± SE) across latitudinal and longitudinal gradients.

https://doi.org/10.5194/essd-2026-720
Preprint. Discussion started: 9 November 2026
© Author(s) 2026. CC BY 4.0 License.



As expected from the biomass-to-carbon conversion procedure, the spatial distribution of AGCd closely followed that of AGBd (Fig. 7b). The highest plot-level values were concentrated in the southern mountain ranges between 39° S and 46° S, reaching 803.1 Mg ha^{-1} of biomass and 394.7 MgC ha^{-1} of carbon. Along the longitudinal gradient, a peak in mean AGCd is observed near 73° W, corresponding to the productive ecosystems of the Coastal Range. Moving eastward, a carbon 'valley' appears, reflecting the scarcity of forest cover in the heavily modified Central Valley of Chile. A subsequent increase near 72° W corresponds to the dense, high-biomass forests of the Andes Mountains. Finally, in the easternmost extent, the longitudinal gradient encompasses the latitudinal overlap of the structurally constrained forests of the Mediterranean ecoregion and the high-biomass *Nothofagus* forests of southern and subantarctic latitudes.

Across the elevational gradient (Fig. 8a), forest carbon stocks display a consistent distribution from sea level up to 1,800 m a.s.l., with mean AGCd values fluctuating between 75 and 100 MgC ha^{-1}. Beyond 1,800 m a.s.l., mean carbon densities drop below 20 MgC ha^{-1}, corresponding to the upper treeline and restrictive environmental conditions for forest development. Regarding slope (Fig. 8b), terrain steepness does not act as a primary limiting factor for carbon accumulation. Mean AGCd reaches a maximum near 105 MgC ha^{-1} at a 10 % gradient and remains between 60 and 90 MgC ha^{-1} across steeper slopes, maintaining a mean near 85 MgC ha^{-1} on gradients between 80 % and 100 %. Although topographic inaccessibility has been traditionally identified as a key factor in the persistence of old-growth forest remnants due to reduced human pressure and limited access for commercial exploitation (Armesto et al., 2009; Miranda et al., 2015), this refugia pattern is not observed as a dominant trend at the national scale in our dataset. This suggests that while topographic barriers may promote localized carbon hotspots by preventing logging and land-use conversion, such effects are likely masked at the national level by the broad heterogeneity of Chilean forest types and land-use histories, suggesting that these topographic limits may increasingly fail to serve as effective barriers to human pressure in the future.



https://doi.org/10.5194/essd-2026-720
Preprint. Discussion started: 9 November 2026
© Author(s) 2026. CC BY 4.0 License.



Figure 8. Variation of aboveground carbon density (AGCd, MgC ha^{-1}) across (a) elevation and (b) slope gradients in Chile's native forests. The circular marker inside each boxplot indicates the mean of AGCd. Scattered gray points represent the individual plot-level estimates to illustrate the underlying data distribution.

Finally, the reliability of plot-level estimates was evaluated through the propagated uncertainties, revealing a distinct gradient in error magnitude governed by the proportion of predictions derived from the BRT model (Fig. A1). Field plots relying entirely on species-specific allometries (Tier 1: 100% allometry-based) exhibited the highest precision, characterized by near-imperceptible confidence intervals across the entire carbon stock range. As reliance on BRT-assisted estimates increased, the uncertainty envelope expanded progressively: plots with low model assistance retained tight confidence bands, whereas plots with higher model dependency exhibited substantially wider confidence intervals and heteroscedastic error behavior in high-density stocks (Fig. A1)

4. Data Usage Notes

The dataset presented here represents a critical shift from historical forest monitoring, which was traditionally designed to quantify commercial timber volume for a limited number of high-value species. The scientific effort invested in measuring trees for a single commercial species often exceeds the total number of trees used to calibrate biomass models for entire tropical regions (Picard et al., 2012). This commercial bias has left a substantial data gap for non-commercial species.

While indirect estimates based on existing allometric models provide a starting point, their accuracy is frequently constrained by the inherent spatial variability of native forests and the practical and legal limitations of destructive sampling for long-lived or protected species (Vann et al., 1998; Weiskittel et al., 2015). Although emerging technologies such as terrestrial LiDAR offer a promising non-destructive path for future allometric refinement, their success depends entirely on the availability of robust, large-scale field baselines like the one provided in this study.

Our field plot database captures biomass stock densities across a broad environmental gradient, providing an extensive field-based reference for national and global applications. At the international scale, the data can support calibration and validation of spaceborne missions, such as NASA's GEDI (Dubayah et al., 2020), ESA's BIOMASS (Le Toan et al., 2011), and NASA-ISRO's NISAR (Rosen et al., 2025), particularly in high-biomass temperate and subantarctic forests where global remote sensing signals frequently saturate (Mutanga et al., 2023). At the national level, the resource can contribute to greenhouse-gas inventory development, NDC assessment and long-term monitoring of forest carbon stocks, advancing the national strategy toward carbon neutrality while providing a foundation to monitor forest resilience under ongoing climate change.

To effectively leverage the dataset for these applications, users must account for the methodological origin of the plot-level estimates when interpreting the associated uncertainties (Holdaway et al., 2014; Li et al., 2022). To facilitate this, we have provided explicit 'Quality Flags' within the dataset that detail the derivation history of each plot. Specifically, these metrics report the exact proportion of AGB calculated directly from species-specific allometric equations versus the proportion imputed via the BRT assistant model. Consequently, these quality metrics allow researchers to filter or weight the data according to their specific operational scale. For highly sensitive, localized analyses where precision is paramount, users can prioritize field plots with a high percentage of allometric-based estimations to minimize model-induced uncertainty.

https://doi.org/10.5194/essd-2026-720
Preprint. Discussion started: 9 November 2026
© Author(s) 2026. CC BY 4.0 License.



For broader regional applications, the complete dataset can be used while explicitly accounting for the plot-level standard errors and confidence intervals provided.

5 Appendices

Table A1. Crosswalk linking traditional Chilean forest types and subtypes with globally recognized Plant Functional Types (PFT).

Plant Functional Types	Chilean forest type	Chilean forest subtype
Needle-leaf evergreen	Alerce	
	Araucaria	
	Ciprés de la Cordillera	
	Ciprés de las Guaitecas	
Broadleaf evergreen	Coihue de Magallanes	
	Coihue - Raulí - Tepa	Coihue
	Coihue - Raulí - Tepa	Coihue - Tepa
	Esclerófilo	
	Palma chilena	
	Roble - Raulí - Coihue	Coihue
	Siempreverde	
Broadleaf deciduous	Coihue - Raulí - Tepa	Coihue - Raulí - Tepa
	Lenga	
	Roble - Hualo	
	Roble - Raulí - Coihue	Roble - Raulí - Coihue
	Roble - Raulí - Coihue	Roble

Table A2. Performance metrics of the diameter-height models used for tree height estimation in individuals without direct measurements.

D-H model	R^2	RMSE
Model 1	0.847	2.48
Model 2	0.604	3.98
Model 3	0.745	1.39
Model 4	0.654	1.62

https://doi.org/10.5194/essd-2026-720
Preprint. Discussion started: 9 November 2026
© Author(s) 2026. CC BY 4.0 License.



Open Access Earth System Science Data Discussions

Table A3. Descriptive statistics of aboveground biomass (Mg ha^{-1}) categorized by Plant Functional Type [27] and forest stand development for the sampled plots. Kruskal-Wallis test results (*H* and *p-values*) indicate the significance of differences in biomass among stand development within each functional type.

Plant Functional Type	Stand development	n	Mean[a] ± SE	Mean[b] AGCd	Min[a]	Max[a]	*H*	*p-value*
Broadleaf deciduous	Primary	192	266 ± 12	128	5.1	753		
	Intermediate	217	176 ± 9	84	2	681.8	85.15	< 0.01
	Secondary	236	127 ± 7	58.7	0.8	686.1		
Broadleaf evergreen	Primary	374	291 ± 9	130.7	1.1	767.7		
	Intermediate	351	196 ± 9	88.4	2.3	762.5	223.45	< 0.01
	Secondary	467	122 ± 6	54.7	0.8	726		
Needle-leaf evergreen	Primary	65	235 ± 23	111.9	0.9	803.1		
	Intermediate	62	218 ± 22	102.5	2.9	704.7	30.22	< 0.01
	Secondary	60	97 ± 14	45.5	1.7	600.2		

[a] Refers to aboveground biomass density (Mg ha^{-1})
[b] Refers to aboveground carbon density (MgC ha^{-1})

473

Table A4. Descriptive statistics of aboveground biomass (Mg ha^{-1}) categorized by ecoregions [31] and forest stand development for the sampled plots. Kruskal-Wallis test results (*H* and *p-values*) indicate the significance of differences in biomass among stand development within each functional type.

Ecoregion	Stand development	n	Mean[a] ± SE	Mean[b] AGCd	Min[a]	Max[a]	*H*	*p-value*
Chilean matorral	Primary	18	25 ± 10	12.1	1.1	153.9		
	Intermediate	33	46 ± 10	21.4	2.3	226.8	7.88	0.02
	Secondary	102	49 ± 7	22.4	0.8	434.1		
Valdivian temperate	Primary	514	295 ± 8	134.4	0.9	803.1		
	Intermediate	520	199 ± 7	91	2	762.5	293.77	< 0.01
	Secondary	610	132 ± 5	59.6	0.8	726		
Magellanic subantartic	Primary	99	233 ± 16	115.2	5.1	753		
	Intermediate	77	200 ± 16	98	2.9	650.4	13.34	< 0.01
	Secondary	51	139 ± 17	68	2.9	503.1		

[a] Refers to aboveground biomass density (Mg ha^{-1})
[b] Refers to aboveground carbon density (MgC ha^{-1})

474

475

476

477

478

479

https://doi.org/10.5194/essd-2026-720
Preprint. Discussion started: 9 November 2026
© Author(s) 2026. CC BY 4.0 License.



Open Access Earth System Science Data Discussions

Table A5. Descriptive statistics of aboveground biomass (Mg ha^{-1}) categorized by Chilean forest type for the sampled plots.

Chilean forest types	n	Mean ± SD	Median	SE	Min	Max
Alerce	47	196 ± 159	156.6	23.3	8.4	649.1
Araucaria	60	311 ± 185	270.2	23.9	1.7	803.1
Ciprés de la Cordillera	21	118 ± 82	115.5	17.8	0.9	297.9
Ciprés de las Guaitecas	59	73 ± 76	48.4	9.9	2.9	425.6
Coihue - Raulí - Tepa	91	307 ± 176	274.2	18.4	9.8	689.9
Coihue de Magallanes	68	286 ± 153	288.4	18.6	25.1	653
Esclerófilo	147	22 ± 29	12.7	2.4	0.8	258.7
Lenga	366	206 ± 162	191.3	8.5	0.8	753
Palma chilena	4	125 ± 104	98.4	52.2	41.6	259.8
Roble - Hualo	93	91 ± 71	69.1	7.4	1.2	336.3
Roble - Raulí - Coihue	416	155 ± 128	117.4	6.3	1.2	763.7
Siempreverde	652	237 ± 169	209.6	6.6	1.7	767.7

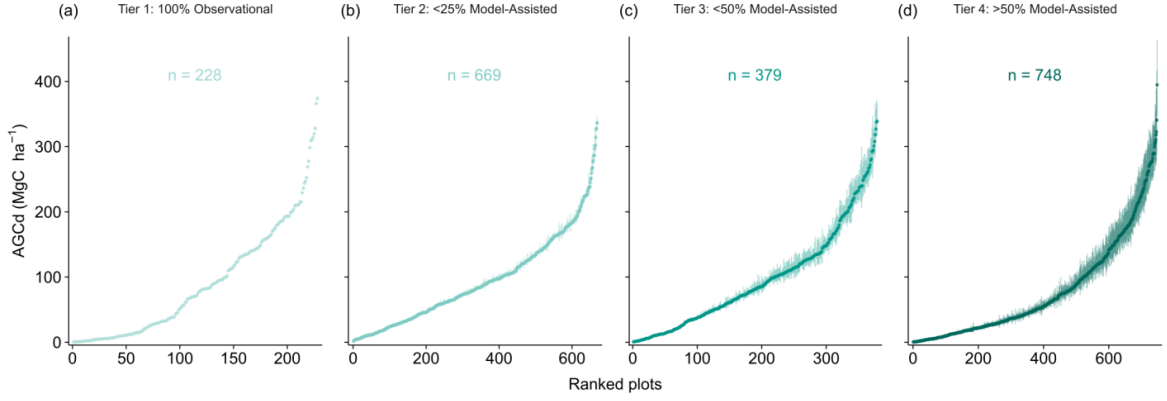


Figure A1. Propagated plot-level uncertainty of aboveground carbon density (AGCd, MgC ha^{-1}) across methodological quality tiers. Field plots are ranked along the x-axis in ascending order of estimated AGCd, where points represent carbon stocks and vertical shaded error bars depict 95 % confidence intervals derived from 1,000 Monte Carlo simulation iterations propagating tree-level errors, BRT model residuals, and carbon fraction conversion uncertainties; (a) Includes plots where 100 % of tree biomass was derived from species-specific allometries, (b) represents low reliance on BRT imputations (< 25 %), (c) corresponds to moderate assistant model dependency (25 – 50 %), and (d) reflects high assistant model dependency (> 50 %).

https://doi.org/10.5194/essd-2026-720
Preprint. Discussion started: 9 November 2026
© Author(s) 2026. CC BY 4.0 License.



Open Access Earth System Science Data Discussions

Data availability

The data supporting the findings of this study are openly available in: https://figshare.com/s/d0fbe20f243bad166846 (Sandoval-Salazar et al., 2026). The repository comprises four core components: (1) the tree-level dataset containing dasometric measurements for 59,408 living trees; (2) a technical parameters dataset encompassing species-specific allometric equations, wood density values, and carbon fraction conversion factors linked to their bibliographic sources for application within valid dasometric ranges; (3) a plot-level dataset providing aggregated aboveground biomass density (AGBd, Mg ha^{-1}) and carbon density (AGCd, MgC ha^{-1}) across 2,024 native forest field plots, integrated with geographic coordinates, ecological attributes, propagated standard errors, 95 % confidence intervals, and Quality Flags detailing model dependency; and (4) the reproducible R code used to execute the propagation framework and perform the tree-to-plot data aggregation workflow.

Author contribution

KSS, AM, JHS, RUJ and BMY contributed to the conceptualization of the study. KSS, AM, JHS, RUJ, TT, and BMY developed the methodology and designed the models. KSS conducted formal analysis, while AM, BLY, FP, and CP performed data curation. AM, BMY, FP and CP were responsible for funding acquisition. KSS, AM, JHS, RUJ, TT, CH and BMY prepared the writing and participated in the writing review and editing of the final manuscript.

Acknowledgements

We acknowledge the Chilean Forest Service (Corporación Nacional Forestal, CONAF) for providing the forest inventory datasets and for their logistical support in plot establishment. We particularly acknowledge the dedication of CONAF's staff and park rangers, whose field-based data collection was essential to this research. BMY and JHS. acknowledge support from the European Union's Horizon 2020 Research and Innovation Programme under the Marie Skłodowska-Curie grant agreement No. 101007950 (DecisionES). AM and RUJ. acknowledge funding from the ANID/FONDEF IDeA I+D grant ID26I10302. AM also acknowledges funding from ANID/FONDECYT Iniciación 11240356. RUJ. also acknowledges funding from the ANID/FONDECYT Regular Grant 1240500, the Center for Climate and Resilience Research (CR2), based at the University of Chile and funded through the Actividades de Interés Nacional (AIN) program, and the ANID Millennium Science Initiative (Center Code NCN2024_040).

https://doi.org/10.5194/essd-2026-720
Preprint. Discussion started: 9 November 2026
© Author(s) 2026. CC BY 4.0 License.



References

Aguilera-Betti, I., Muñoz, A. A., Stahle, D., Figueroa, G., Duarte, F., González-Reyes, Á., Christie, D., Lara, A., González, M. E., Sheppard, P. R., Sauchyn, D., Moreira-Muñoz, A., Toledo-Guerrero, I., Olea, M., Apaz, P., and Fernandez, A.: The First Millennium-Age *Araucaria Araucana* in Patagonia, Tree-Ring Research, 73, 53–56, https://doi.org/10.3959/1536-1098-73.1.53, 2017.

Altamirano, A., Schlegel, B., Thiers, Ó., Miranda, A., Pilquinao, B., Orrego, R., and Rocha, C.: Disponibilidad y potencial energético de la biomasa del bosque nativo para el desarrollo de la dendroenergía en el centro-sur de Chile, Bosque (Valdivia), 36, 223–237, https://doi.org/10.4067/S0717-92002015000200008, 2015.

Armesto, J. J., Smith-Ramírez, C., Carmona, M. R., Celis-Diez, J. L., Díaz, I. A., Gaxiola, A., Gutiérrez, A. G., Núñez-Avila, M. C., Pérez, C. A., and Rozzi, R.: Old-Growth Temperate Rainforests of South America: Conservation, Plant–Animal Interactions, and Baseline Biogeochemical Processes, in: Old-Growth Forests, vol. 207, edited by: Wirth, C., Gleixner, G., and Heimann, M., Springer Berlin Heidelberg, Berlin, Heidelberg, 367–390, https://doi.org/10.1007/978-3-540-92706-8_16, 2009.

Basoa, K., Martínez, R., Carrasco, P., Guzmán, R., Soto, I., González, M. D., Beltrán, I., Salazar, F., Ricciardi, C., Cornejo, P., Rojas Ponce, Y., Sagardía Parga, R., Bahamóndez, C., Martin, M., Albornoz, A., Becar, N., Trujillo, G., Pincheira, F., Huss, E., Avilés, M., Valdés, J. M., Campos, B., Contreras, C., Martínez, G., and Ocampo, H.: Documento del inventario nacional de gases de efecto invernadero Serie 1990-2022, Ministerio del Medio Ambiente, 2024.

Chave, J., Condit, R., Aguilar, S., Hernandez, A., Lao, S., and Perez, R.: Error propagation and scaling for tropical forest biomass estimates, Phil. Trans. R. Soc. Lond. B, 359, 409–420, https://doi.org/10.1098/rstb.2003.1425, 2004.

Chave, J., Réjou-Méchain, M., Búrquez, A., Chidumayo, E., Colgan, M. S., Delitti, W. B. C., Duque, A., Eid, T., Fearnside, P. M., Goodman, R. C., Henry, M., Martínez-Yrízar, A., Mugasha, W. A., Muller-Landau, H. C., Mencuccini, M., Nelson, B. W., Ngomanda, A., Nogueira, E. M., Ortiz-Malavassi, E., Pélissier, R., Ploton, P., Ryan, C. M., Saldarriaga, J. G., and Vieilledent, G.: Improved allometric models to estimate the aboveground biomass of tropical trees, Global Change Biology, 20, 3177–3190, https://doi.org/10.1111/gcb.12629, 2014.

CONAF: Manual de operaciones de terreno: Proyecto monitoreo de biomasa y carbono forestal. Sistema de Monitoreo Nacional de Biomasa y Carbono Forestal para los recursos forestales localizados desde las regiones de Atacama a Magallanes y la Antártica Chilena, CONAF, Santiago, 2015.

CONAF: Catastro de los Recursos Vegetacionales y Uso de la Tierra de Chile, Departamento de Monitoreo, CONAF, 2025.

Curtis, P. G., Slay, C. M., Harris, N. L., Tyukavina, A., and Hansen, M. C.: Classifying drivers of global forest loss, Science, 361, 1108–1111, https://doi.org/10.1126/science.aau3445, 2018.

Dinerstein, E., Olson, D., Joshi, A., Vynne, C., Burgess, N. D., Wikramanayake, E., Hahn, N., Palminteri, S., Hedao, P., Noss, R., Hansen, M., Locke, H., Ellis, E. C., Jones, B., Barber, C. V., Hayes, R., Kormos, C., Martin, V., Crist, E., Sechrest, W., Price, L., Baillie, J. E. M., Weeden, D., Suckling, K., Davis, C., Sizer, N., Moore, R., Thau, D., Birch, T., Potapov, P., Turubanova, S., Tyukavina, A., De Souza, N., Pintea, L., Brito, J. C., Llewellyn, O. A., Miller, A. G., Patzelt, A., Ghazanfar, S. A., Timberlake, J., Klöser, H., Shennan-Farpón, Y., Kindt, R., Lillesø, J.-P. B., Van Breugel, P., Graudal, L., Voge, M., Al-Shammari, K. F., and Saleem, M.: An Ecoregion-Based Approach to Protecting Half the Terrestrial Realm, BioScience, 67, 534–545, https://doi.org/10.1093/biosci/bix014, 2017.

Donoso, C.: Tipos forestales de los bosques nativos de Chile, Proyecto CONAF/PNUD/FAO., Proyecto CONAF/PNUD/FAO, Santiago, Chile, 70 pp., 1981.

Donoso, C.: Las especies arbóreas de los bosques templados de Chile y Argentina. Autoecología, Segunda edición., 2013.

Donoso, C., Promis, Á., and Coopman, R.: El clima, in: Ecología Forestal. Bases para el Manejo Sustentable y Conservación de los Bosques Nativos de Chile., Ediciones Universidad Austral de Chile, 25–131, 2014.

https://doi.org/10.5194/essd-2026-720
Preprint. Discussion started: 9 November 2026
© Author(s) 2026. CC BY 4.0 License.



569 Dubayah, R., Blair, J. B., Goetz, S., Fatoyinbo, L., Hansen, M., Healey, S., Hofton, M., Hurtt, G., Kellner, J., Luthcke, S.,
570 Armston, J., Tang, H., Duncanson, L., Hancock, S., Jantz, P., Marselis, S., Patterson, P. L., Qi, W., and Silva, C.: The Global
571 Ecosystem Dynamics Investigation: High-resolution laser ranging of the Earth's forests and topography, Science of
572 Remote Sensing, 1, 100002, https://doi.org/10.1016/j.srs.2020.100002, 2020.

573 Enquist, B. J., West, G. B., Charnov, E. L., and Brown, J. H.: Allometric scaling of production and life-history variation in
574 vascular plants, Nature, 401, 907–911, https://doi.org/10.1038/44819, 1999.

575 European Space Agency: Copernicus Global Digital Elevation Model, https://doi.org/10.5069/G9028PQB, 2024.

576 Fajardo, A. and Piper, F. I.: Intraspecific trait variation and covariation in a widespread tree species (Nothofagus pumilio)
577 in southern Chile, New Phytologist, 189, 259–271, https://doi.org/10.1111/j.1469-8137.2010.03468.x, 2011.

578 FAO: El estado de los bosques del mundo 2024, FAO, https://doi.org/10.4060/cd1211es, 2024.

579 Franklin, J. F., Spies, T. A., Pelt, R. V., Carey, A. B., Thornburgh, D. A., Berg, D. R., Lindenmayer, D. B., Harmon, M. E.,
580 Keeton, W. S., Shaw, D. C., Bible, K., and Chen, J.: Disturbances and structural development of natural forest ecosystems
581 with silvicultural implications, using Douglas-fir forests as an example, Forest Ecology and Management, 155, 399–423,
582 https://doi.org/10.1016/S0378-1127(01)00575-8, 2002.

583 Friedlingstein, P., O'Sullivan, M., Jones, M. W., Andrew, R. M., Bakker, D. C. E., Hauck, J., Landschützer, P., Le Quéré, C., Li,
584 H., Luijkx, I. T., Peters, G. P., Peters, W., Pongratz, J., Schwingshackl, C., Sitch, S., Canadell, J. G., Ciais, P., Aas, K., Alin, S.
585 R., Anthoni, P., Barbero, L., Bates, N. R., Bellouin, N., Benoit-Cattin, A., Berghoff, C. F., Bernardello, R., Bopp, L., Brasika, I.
586 B. M., Chamberlain, M. A., Chandra, N., Chevallier, F., Chini, L. P., Collier, N. O., Colligan, T. H., Cronin, M., Djeutchouang,
587 L., Dou, X., Enright, M. P., Enyo, K., Erb, M., Evans, W., Feely, R. A., Feng, L., Ford, D. J., Foster, A., Fransner, F., Gasser, T.,
588 Gehlen, M., Gkritzalis, T., Goncalves De Souza, J., Grassi, G., Gregor, L., Gruber, N., Guenet, B., Gürses, Ö., Harrington, K.,
589 Harris, I., Heinke, J., Hurtt, G. C., Iida, Y., Ilyina, T., Ito, A., Jacobson, A. R., Jain, A. K., Jarníková, T., Jersild, A., Jiang, F.,
590 Jones, S. D., Kato, E., Keeling, R. F., Klein Goldewijk, K., Knauer, J., Kong, Y., Korsbakken, J. I., Koven, C., Kunimitsu, T., Lan,
591 X., Liu, J., Liu, Z., Liu, Z., Lo Monaco, C., Ma, L., Marland, G., McGuire, P. C., McKinley, G. A., Melton, J., Monacci, N.,
592 Monier, E., Morgan, E. J., Munro, D. R., Müller, J. D., Nakaoka, S.-I., Nayagam, L. R., Niwa, Y., Nutzel, T., Olsen, A., Omar, A.
593 M., Pan, N., Pandey, S., et al.: Global Carbon Budget 2025, https://doi.org/10.5194/essd-2025-659, 13 November 2025.

594 Friedman, J. H.: Greedy function approximation: A gradient boosting machine., Ann. Statist., 29,
595 https://doi.org/10.1214/aos/1013203451, 2001.

596 Gayoso, J. and Guerra, J.: Contenido de carbono en la biomasa aérea de bosques nativos en Chile, Bosque (Valdivia), 26,
597 https://doi.org/10.4067/S0717-92002005000200005, 2005.

598 Gayoso, J., Guerra, Javier, and Alarcón, Diego: Medición de la capacidad de captura de carbono en bosques de Chile y
599 promoción en el mercado mundial: Contenido de carbono y funciones de biomasa en especies nativas y exóticas.,
600 2002.

601 Gómez-González, S., Miranda, A., Hoyos-Santillan, J., Lara, A., Moraga, P., and Pausas, J. G.: Afforestation and climate
602 mitigation: lessons from Chile, Trends in Ecology & Evolution, 39, 5–8, https://doi.org/10.1016/j.tree.2023.09.014, 2024.

603 González, M., Lara, A., Urrutia-Jalabert, R., Bustos-Salazar, A., Ruiz-Gómez, C., and Aravena, J. C.: Carbon stocks across
604 different environments, disturbance regimes, and stand age in Fitzroya cupressoides forests, the longest-lived species of
605 the southern hemisphere, Front. For. Glob. Change, 5, 960429, https://doi.org/10.3389/ffgc.2022.960429, 2022.

606 González, M., Miranda, A., Urrutia-Jalabert, R., Zamorano-Elgueta, C., Ibarra, C., Pogorelow, B., and Lara, A.: Bosques
607 nativos, in: Informe País 2025, Universidad de Chile, Santiago, Chile, 2026.

608 Griscom, B. W., Adams, J., Ellis, P. W., Houghton, R. A., Lomax, G., Miteva, D. A., Schlesinger, W. H., Shoch, D., Siikamäki,
609 J. V., Smith, P., Woodbury, P., Zganjar, C., Blackman, A., Campari, J., Conant, R. T., Delgado, C., Elias, P., Gopalakrishna,
610 T., Hamsik, M. R., Herrero, M., Kiesecker, J., Landis, E., Laestadius, L., Leavitt, S. M., Minnemeyer, S., Polasky, S., Potapov,
611 P., Putz, F. E., Sanderman, J., Silvius, M., Wollenberg, E., and Fargione, J.: Natural climate solutions, Proc. Natl. Acad. Sci.
612 U.S.A., 114, 11645–11650, https://doi.org/10.1073/pnas.1710465114, 2017.

https://doi.org/10.5194/essd-2026-720
Preprint. Discussion started: 9 November 2026
© Author(s) 2026. CC BY 4.0 License.



Harris, D. J., Ndolo Ebika, S. T., Sanz, C. M., Madingou, M. P. N., and Morgan, D. B.: Large trees in tropical rain forests require big plots, Plants People Planet, 3, 282–294, https://doi.org/10.1002/ppp3.10194, 2021.

Hijmans, R., Phillips, S., Leathwick, J., and Elith, J.: dismo: Species Distribution Modeling, https://doi.org/10.32614/CRAN.package.dismo, 2023.

Holdaway, R. J., McNeill, S. J., Mason, N. W. H., and Carswell, F. E.: Propagating Uncertainty in Plot-based Estimates of Forest Carbon Stock and Carbon Stock Change, Ecosystems, 17, 627–640, https://doi.org/10.1007/s10021-014-9749-5, 2014.

Houghton, R. A. and Nassikas, A. A.: Global and regional fluxes of carbon from land use and land cover change 1850–2015, Global Biogeochemical Cycles, 31, 456–472, https://doi.org/10.1002/2016GB005546, 2017.

Houghton, R. A., Hall, F., and Goetz, S. J.: Importance of biomass in the global carbon cycle, J. Geophys. Res., 114, 2009JG000935, https://doi.org/10.1029/2009JG000935, 2009.

Hurtado, F.: Funciones locales de volumen de especies nativas de bosques naturales y plantaciones. Región de Valparaíso, 2012.

IPCC: Climate Change and Land. An IPCC Special Report on climate change, desertification, land degradation, sustainable land management, food security, and greenhouse gas fluxes in terrestrial ecosystems, Ginebra, Suiza, 2019.

IPCC: Climate Change 2023: Synthesis Report. Summary for Policymakers, Intergovernmental Panel on Climate Change, 2023.

Jucker, T., Caspersen, J., Chave, J., Antin, C., Barbier, N., Bongers, F., Dalponte, M., Van Ewijk, K. Y., Forrester, D. I., Haeni, M., Higgins, S. I., Holdaway, R. J., Iida, Y., Lorimer, C., Marshall, P. L., Momo, S., Moncrieff, G. R., Ploton, P., Poorter, L., Rahman, K. A., Schlund, M., Sonké, B., Sterck, F. J., Trugman, A. T., Usoltsev, V. A., Vanderwel, M. C., Waldner, P., Wedeux, B. M. M., Wirth, C., Wöll, H., Woods, M., Xiang, W., Zimmermann, N. E., and Coomes, D. A.: Allometric equations for integrating remote sensing imagery into forest monitoring programmes, Global Change Biology, 23, 177–190, https://doi.org/10.1111/gcb.13388, 2017.

Kassambara, A.: rstatix: Pipe-Friendly Framework for Basic Statistical Tests, https://doi.org/10.32614/CRAN.package.rstatix, 2019.

Keith, H., Mackey, B. G., and Lindenmayer, D. B.: Re-evaluation of forest biomass carbon stocks and lessons from the world's most carbon-dense forests, Proc. Natl. Acad. Sci. U.S.A., 106, 11635–11640, https://doi.org/10.1073/pnas.0901970106, 2009.

Körner, C.: Alpine Treelines, Springer Basel, Basel, https://doi.org/10.1007/978-3-0348-0396-0, 2012.

Lara, A., Amoroso, M., Bannister, J., Donoso, C., González, M., Vargas, R., Smith-Ramírez, C., Arellano, G., and Gutiérrez, A. G.: Sucesión y Dinámica de Bosques Templados en Chile, in: Ecología Forestal. Bases para el Manejo Sustentable y Conservación de los Bosques Nativos de Chile, Ediciones Uach, 323–410, 2014.

Le Toan, T., Quegan, S., Davidson, M. W. J., Balzter, H., Paillou, P., Papathanassiou, K., Plummer, S., Rocca, F., Saatchi, S., Shugart, H., and Ulander, L.: The BIOMASS mission: Mapping global forest biomass to better understand the terrestrial carbon cycle, Remote Sensing of Environment, 115, 2850–2860, https://doi.org/10.1016/j.rse.2011.03.020, 2011.

Lewis, S. L., Sonké, B., Sunderland, T., Begne, S. K., Lopez-Gonzalez, G., Van Der Heijden, G. M. F., Phillips, O. L., Affum-Baffoe, K., Baker, T. R., Banin, L., Bastin, J.-F., Beeckman, H., Boeckx, P., Bogaert, J., De Cannière, C., Chezeaux, E., Clark, C. J., Collins, M., Djagbletey, G., Djuikouo, M. N. K., Droissart, V., Doucet, J.-L., Ewango, C. E. N., Fauset, S., Feldpausch, T. R., Foli, E. G., Gillet, J.-F., Hamilton, A. C., Harris, D. J., Hart, T. B., De Haulleville, T., Hladik, A., Hufkens, K., Huygens, D., Jeanmart, P., Jeffery, K. J., Kearsley, E., Leal, M. E., Lloyd, J., Lovett, J. C., Makana, J.-R., Malhi, Y., Marshall, A. R., Ojo, L., Peh, K. S.-H., Pickavance, G., Poulsen, J. R., Reitsma, J. M., Sheil, D., Simo, M., Steppe, K., Taedoumg, H. E., Talbot, J., Taplin, J. R. D., Taylor, D., Thomas, S. C., Toirambe, B., Verbeeck, H., Vleminckx, J., White, L. J. T., Willcock, S., Woell, H.,

https://doi.org/10.5194/essd-2026-720
Preprint. Discussion started: 9 November 2026
© Author(s) 2026. CC BY 4.0 License.



and Zemagho, L.: Above-ground biomass and structure of 260 African tropical forests, Phil. Trans. R. Soc. B, 368, 20120295, https://doi.org/10.1098/rstb.2012.0295, 2013.

Li, Z., Bi, S., Hao, S., and Cui, Y.: Aboveground biomass estimation in forests with random forest and Monte Carlo-based uncertainty analysis, Ecological Indicators, 142, 109246, https://doi.org/10.1016/j.ecolind.2022.109246, 2022.

Lutz, J. A., Furniss, T. J., Johnson, D. J., Davies, S. J., Allen, D., Alonso, A., Anderson-Teixeira, K. J., Andrade, A., Baltzer, J., Becker, K. M. L., Blomdahl, E. M., Bourg, N. A., Bunyavejchewin, S., Burslem, D. F. R. P., Cansler, C. A., Cao, K., Cao, M., Cárdenas, D., Chang, L., Chao, K., Chao, W., Chiang, J., Chu, C., Chuyong, G. B., Clay, K., Condit, R., Cordell, S., Dattaraja, H. S., Duque, A., Ewango, C. E. N., Fischer, G. A., Fletcher, C., Freund, J. A., Giardina, C., Germain, S. J., Gilbert, G. S., Hao, Z., Hart, T., Hau, B. C. H., He, F., Hector, A., Howe, R. W., Hsieh, C., Hu, Y., Hubbell, S. P., Inman-Narahari, F. M., Itoh, A., Janík, D., Kassim, A. R., Kenfack, D., Korte, L., Král, K., Larson, A. J., Li, Y., Lin, Y., Liu, S., Lum, S., Ma, K., Makana, J., Malhi, Y., McMahon, S. M., McShea, W. J., Memiaghe, H. R., Mi, X., Morecroft, M., Musili, P. M., Myers, J. A., Novotny, V., De Oliveira, A., Ong, P., Orwig, D. A., Ostertag, R., Parker, G. G., Patankar, R., Phillips, R. P., Reynolds, G., Sack, L., Song, G. M., Su, S., Sukumar, R., Sun, I., Suresh, H. S., Swanson, M. E., Tan, S., Thomas, D. W., Thompson, J., Uriarte, M., Valencia, R., Vicentini, A., Vrška, T., Wang, X., Weiblen, G. D., Wolf, A., Wu, S., Xu, H., Yamakura, T., Yap, S., and Zimmerman, J. K.: Global importance of large-diameter trees, Global Ecol Biogeogr, 27, 849–864, https://doi.org/10.1111/geb.12747, 2018.

Luyssaert, S., Schulze, E.-D., Börner, A., Knohl, A., Hessenmöller, D., Law, B. E., Ciais, P., and Grace, J.: Old-growth forests as global carbon sinks, Nature, 455, 213–215, https://doi.org/10.1038/nature07276, 2008.

Ma, H., Crowther, T. W., Mo, L., Maynard, D. S., Renner, S. S., Van Den Hoogen, J., Zou, Y., Liang, J., de-Miguel, S., Nabuurs, G.-J., Reich, P. B., Niinemets, Ü., Abegg, M., Adou Yao, Y. C., Alberti, G., Almeyda Zambrano, A. M., Alvarado, B. V., Alvarez-Dávila, E., Alvarez-Loayza, P., Alves, L. F., Ammer, C., Antón-Fernández, C., Araujo-Murakami, A., Arroyo, L., Avitabile, V., Aymard, G. A., Baker, T. R., Bałazy, R., Banki, O., Barroso, J. G., Bastian, M. L., Bastin, J.-F., Birigazzi, L., Birnbaum, P., Bitariho, R., Boeckx, P., Bongers, F., Bouriaud, O., Brancalion, P. H. S., Brandl, S., Brearley, F. Q., Brienen, R., Broadbent, E. N., Bruelheide, H., Bussotti, F., Cazzolla Gatti, R., César, R. G., Cesljar, G., Chazdon, R., Chen, H. Y. H., Chisholm, C., Cho, H., Cienciala, E., Clark, C., Clark, D., Colletta, G. D., Coomes, D. A., Valverde, F. C., Corral-Rivas, J. J., Crim, P. M., Cumming, J. R., Dayanandan, S., De Gasper, A. L., Decuyper, M., Derroire, G., DeVries, B., Djordjevic, I., Dolezal, J., Dourdain, A., Engone Obiang, N. L., Enquist, B. J., Eyre, T. J., Fandohan, A. B., Fayle, T. M., Feldpausch, T. R., Ferreira, L. V., Finér, L., Fischer, M., Fletcher, C., Fridman, J., Frizzera, L., Gamarra, J. G. P., Gianelle, D., Glick, H. B., Harris, D. J., Hector, A., Hemp, A., Hengeveld, G., Hérault, B., Herbohn, J. L., Herold, M., Hillers, A., Honorio Coronado, E. N., Hui, C., Ibanez, T. T., Amaral, I., Imai, N., Jagodziński, A. M., Jaroszewicz, B., et al.: The global biogeography of tree leaf form and habit, Nat. Plants, 9, 1795–1809, https://doi.org/10.1038/s41477-023-01543-5, 2023.

McDowell, N. G., Allen, C. D., Anderson-Teixeira, K., Aukema, B. H., Bond-Lamberty, B., Chini, L., Clark, J. S., Dietze, M., Grossiord, C., Hanbury-Brown, A., Hurtt, G. C., Jackson, R. B., Johnson, D. J., Kueppers, L., Lichstein, J. W., Ogle, K., Poulter, B., Pugh, T. A. M., Seidl, R., Turner, M. G., Uriarte, M., Walker, A. P., and Xu, C.: Pervasive shifts in forest dynamics in a changing world, Science, 368, eaaz9463, https://doi.org/10.1126/science.aaz9463, 2020.

Mehtätalo, L., de-Miguel, S., and Gregoire, T. G.: Modeling height-diameter curves for prediction, Can. J. For. Res., 45, 826–837, https://doi.org/10.1139/cjfr-2015-0054, 2015.

Milla, F., Emanuelli, P., Sartori, A., and Emanuelli, J.: Compendio de funciones alométricas para la estimación de la biomasa de especies forestales presentes en Chile: Elemento clave para el desarrollo de la Estrategia Nacional de Bosques y Cambio Climático (ENBCC), 2013.

Miranda, A., Altamirano, A., Cayuela, L., Pincheira, F., and Lara, A.: Different times, same story: Native forest loss and landscape homogenization in three physiographical areas of south-central of Chile, Applied Geography, 60, 20–28, https://doi.org/10.1016/j.apgeog.2015.02.016, 2015.

Miranda, A., Altamirano, A., Cayuela, L., Lara, A., and González, M.: Native forest loss in the Chilean biodiversity hotspot: revealing the evidence, Reg Environ Change, 17, 285–297, https://doi.org/10.1007/s10113-016-1010-7, 2017.

https://doi.org/10.5194/essd-2026-720
Preprint. Discussion started: 9 November 2026
© Author(s) 2026. CC BY 4.0 License.



Miranda, A., Hoyos-Santillan, J., Lara, A., Mentler, R., Huertas-Herrera, A., Toro-Manríquez, M. D. R., and Sepulveda-Jauregui, A.: Equivalent impacts of logging and beaver activities on aboveground carbon stock loss in the southernmost forest on Earth, Sci Rep, 13, 18350, https://doi.org/10.1038/s41598-023-45657-4, 2023.

Mittermeier, R., Gil, P., Hoffman, M., Pilgrim, J., Brooks, T., Mittermeier, C., Lamoreux, J., and Fonseca, G.: Hotspots Revisited. Earth's Biologically Richest and Most Endangered Terrestrial Ecoregions, Cemex, Mexico, 2004.

Mutanga, O., Masenyama, A., and Sibanda, M.: Spectral saturation in the remote sensing of high-density vegetation traits: A systematic review of progress, challenges, and prospects, ISPRS Journal of Photogrammetry and Remote Sensing, 198, 297–309, https://doi.org/10.1016/j.isprsjprs.2023.03.010, 2023.

Myers, N., Mittermeier, R. A., Mittermeier, C. G., Da Fonseca, G. A. B., and Kent, J.: Biodiversity hotspots for conservation priorities, Nature, 403, 853–858, https://doi.org/10.1038/35002501, 2000.

Noon, M. L., Goldstein, A., Ledezma, J. C., Roehrdanz, P. R., Cook-Patton, S. C., Spawn-Lee, S. A., Wright, T. M., Gonzalez-Roglich, M., Hole, D. G., Rockström, J., and Turner, W. R.: Mapping the irrecoverable carbon in Earth's ecosystems, Nat Sustain, 5, 37–46, https://doi.org/10.1038/s41893-021-00803-6, 2021.

Pan, Y., Birdsey, R. A., Phillips, O. L., and Jackson, R. B.: The Structure, Distribution, and Biomass of the World's Forests, Annu. Rev. Ecol. Evol. Syst., 44, 593–622, https://doi.org/10.1146/annurev-ecolsys-110512-135914, 2013.

Picard, N., Saint-André, L., and Henry, M.: Manual for building tree volume and biomass allometric equations: from filed measurement to prediction, Food and Agriculture Organization of the United Nations (FA0) [u.a.], Rome, 207 pp., 2012.

Pinheiro, J., Bates, D., and R Core Team: nlme: Linear and Nonlinear Mixed Effects Models, 2023.

Piper, F. I., Viñegla, B., Linares, J. C., Camarero, J. J., Cavieres, L. A., and Fajardo, A.: Mediterranean and temperate treelines are controlled by different environmental drivers, Journal of Ecology, 104, 691–702, https://doi.org/10.1111/1365-2745.12555, 2016.

Réjou-Méchain, M., Muller-Landau, H. C., Detto, M., Thomas, S. C., Le Toan, T., Saatchi, S. S., Barreto-Silva, J. S., Bourg, N. A., Bunyavejchewin, S., Butt, N., Brockelman, W. Y., Cao, M., Cárdenas, D., Chiang, J.-M., Chuyong, G. B., Clay, K., Condit, R., Dattaraja, H. S., Davies, S. J., Duque, A., Esufali, S., Ewango, C., Fernando, R. H. S., Fletcher, C. D., Gunatilleke, I. A. U. N., Hao, Z., Harms, K. E., Hart, T. B., Hérault, B., Howe, R. W., Hubbell, S. P., Johnson, D. J., Kenfack, D., Larson, A. J., Lin, L., Lin, Y., Lutz, J. A., Makana, J.-R., Malhi, Y., Marthews, T. R., McEwan, R. W., McMahon, S. M., McShea, W. J., Muscarella, R., Nathalang, A., Noor, N. S. M., Nytch, C. J., Oliveira, A. A., Phillips, R. P., Pongpattananurak, N., Punchi-Manage, R., Salim, R., Schurman, J., Sukumar, R., Suresh, H. S., Suwanvecho, U., Thomas, D. W., Thompson, J., Uríarte, M., Valencia, R., Vicentini, A., Wolf, A. T., Yap, S., Yuan, Z., Zartman, C. E., Zimmerman, J. K., and Chave, J.: Local spatial structure of forest biomass and its consequences for remote sensing of carbon stocks, Biogeosciences, 11, 6827–6840, https://doi.org/10.5194/bg-11-6827-2014, 2014.

Ridgeway, G., Edwards, D., Kriegler, B., Schroedl, S., Southworth, H., Greenwell, B., Boehmke, B., and Cunningham, J.: gbm: Generalized Boosted Regression Models, https://doi.org/10.32614/CRAN.package.gbm, 2003.

Rosen, P. A., Bawden, G. W., Barela, P., Chapman, B., Fattahi, H., Jones, C. E., Joughin, I. R., Lavalle, M., Lohman, R. B., Simons, M., Siqueira, P., Das, A., Desai, N. M., Kumar, R., Putrevu, D., Sharma, R., and Shrikant, C.: The NASA-ISRO SAR Mission: A summary, IEEE Geosci. Remote Sens. Mag., 13, 8–34, https://doi.org/10.1109/MGRS.2025.3578258, 2025.

Sandoval-Salazar, K., Miranda, A., Hoyos-Santillan, J., Urrutia-Jalabert, R., Tokola, T., Hormazabal, C., Pincheira, F., Pérez, C., and Mola-Yudego, B.: Plot-level estimates of living trees carbon stocks in Chilean native forests, 2026.

Sardans, J. and Peñuelas, J.: Plant-soil interactions in Mediterranean forest and shrublands: impacts of climatic change, Plant Soil, 365, 1–33, https://doi.org/10.1007/s11104-013-1591-6, 2013.

Schlegel, B.: Estimación de la biomasa y carbono en bosques del tipo forestal siempreverde, 1–13, 2001.

https://doi.org/10.5194/essd-2026-720
Preprint. Discussion started: 9 November 2026
© Author(s) 2026. CC BY 4.0 License.



741 Seddon, N., Daniels, E., Davis, R., Chausson, A., Harris, R., Hou-Jones, X., Huq, S., Kapos, V., Mace, G. M., Rizvi, A. R.,
742 Reid, H., Roe, D., Turner, B., and Wicander, S.: Global recognition of the importance of nature-based solutions to the
743 impacts of climate change, Glob. Sustain., 3, e15, https://doi.org/10.1017/sus.2020.8, 2020.

744 Seidl, R., Thom, D., Kautz, M., Martin-Benito, D., Peltoniemi, M., Vacchiano, G., Wild, J., Ascoli, D., Petr, M., Honkaniemi,
745 J., Lexer, M. J., Trotsiuk, V., Mairota, P., Svoboda, M., Fabrika, M., Nagel, T. A., and Reyer, C. P. O.: Forest disturbances
746 under climate change, Nature Clim Change, 7, 395–402, https://doi.org/10.1038/nclimate3303, 2017.

747 Slik, J. W. F., Paoli, G., McGuire, K., Amaral, I., Barroso, J., Bastian, M., Blanc, L., Bongers, F., Boundja, P., Clark, C.,
748 Collins, M., Dauby, G., Ding, Y., Doucet, J., Eler, E., Ferreira, L., Forshed, O., Fredriksson, G., Gillet, J., Harris, D., Leal, M.,
749 Laumonier, Y., Malhi, Y., Mansor, A., Martin, E., Miyamoto, K., Araujo-Murakami, A., Nagamasu, H., Nilus, R., Nurtjahya,
750 E., Oliveira, Á., Onrizal, O., Parada-Gutierrez, A., Permana, A., Poorter, L., Poulsen, J., Ramirez-Angulo, H., Reitsma, J.,
751 Rovero, F., Rozak, A., Sheil, D., Silva-Espejo, J., Silveira, M., Spironelo, W., Ter Steege, H., Stevart, T., Navarro-Aguilar, G.
752 E., Sunderland, T., Suzuki, E., Tang, J., Theilade, I., Van Der Heijden, G., Van Valkenburg, J., Van Do, T., Vilanova, E., Vos, V.,
753 Wich, S., Wöll, H., Yoneda, T., Zang, R., Zhang, M., and Zweifel, N.: Large trees drive forest aboveground biomass variation
754 in moist lowland forests across the tropics, Global Ecology and Biogeography, 22, 1261–1271,
755 https://doi.org/10.1111/geb.12092, 2013.

756 Soto, D. P., Salas, C., Donoso, P. J., and Uteau, D.: Heterogeneidad estructural y espacial de un bosque mixto dominado
757 por Nothofagus dombeyi después de un disturbio parcial, Rev. chil. hist. nat., 83, https://doi.org/10.4067/S0716-
758 078X2010000300002, 2010.

759 Sullivan, M. J. P., Talbot, J., Lewis, S. L., Phillips, O. L., Qie, L., Begne, S. K., Chave, J., Cuni-Sanchez, A., Hubau, W., Lopez-
760 Gonzalez, G., Miles, L., Monteagudo-Mendoza, A., Sonké, B., Sunderland, T., Ter Steege, H., White, L. J. T., Affum-Baffoe,
761 K., Aiba, S., De Almeida, E. C., De Oliveira, E. A., Alvarez-Loayza, P., Dávila, E. Á., Andrade, A., Aragão, L. E. O. C., Ashton,
762 P., Aymard C., G. A., Baker, T. R., Balinga, M., Banin, L. F., Baraloto, C., Bastin, J.-F., Berry, N., Bogaert, J., Bonal, D.,
763 Bongers, F., Brienen, R., Camargo, J. L. C., Cerón, C., Moscoso, V. C., Chezeaux, E., Clark, C. J., Pacheco, Á. C., Comiskey,
764 J. A., Valverde, F. C., Coronado, E. N. H., Dargie, G., Davies, S. J., De Canniere, C., Djuikouo K., M. N., Doucet, J.-L., Erwin,
765 T. L., Espejo, J. S., Ewango, C. E. N., Fauset, S., Feldpausch, T. R., Herrera, R., Gilpin, M., Gloor, E., Hall, J. S., Harris, D. J.,
766 Hart, T. B., Kartawinata, K., Kho, L. K., Kitayama, K., Laurance, S. G. W., Laurance, W. F., Leal, M. E., Lovejoy, T., Lovett, J.
767 C., Lukasu, F. M., Makana, J.-R., Malhi, Y., Maracahipes, L., Marimon, B. S., Junior, B. H. M., Marshall, A. R., Morandi, P. S.,
768 Mukendi, J. T., Mukinzi, J., Nilus, R., Vargas, P. N., Camacho, N. C. P., Pardo, G., Peña-Claros, M., Pétronelli, P.,
769 Pickavance, G. C., Poulsen, A. D., Poulsen, J. R., Primack, R. B., Priyadi, H., Quesada, C. A., Reitsma, J., Réjou-Méchain,
770 M., Restrepo, Z., Rutishauser, E., Salim, K. A., Salomão, R. P., Samsoedin, I., Sheil, D., et al.: Diversity and carbon storage
771 across the tropical forest biome, Sci Rep, 7, 39102, https://doi.org/10.1038/srep39102, 2017.

772 Urrutia-Jalabert, R., Malhi, Y., and Lara, A.: The Oldest, Slowest Rainforests in the World? Massive Biomass and Slow
773 Carbon Dynamics of Fitzroya cupressoides Temperate Forests in Southern Chile, PLoS ONE, 10, e0137569,
774 https://doi.org/10.1371/journal.pone.0137569, 2015.

775 Vann, D. R., Palmiotto, P. A., and Richard Strimbeck, G.: Allometric equations for two South American conifers: Test of a
776 non-destructive method, Forest Ecology and Management, 106, 55–71, https://doi.org/10.1016/S0378-1127(97)00215-6,
777 1998.

778 Veblen, T. T., Young, K. R., and Orme, A. R. (Eds.): The physical geography of South America, Oxford University Press,
779 Oxford ; New York, 361 pp., 2007.

780 Weiskittel, A. R., MacFarlane, D. W., Radtke, P. J., Affleck, D. L. R., Temesgen, H., Woodall, C. W., Westfall, J. A., and
781 Coulston, J. W.: A Call to Improve Methods for Estimating Tree Biomass for Regional and National Assessments, Journal
782 of Forestry, 113, 414–424, https://doi.org/10.5849/jof.14-091, 2015.

783

784

785